6.11 Recommended Readings

Ball, C.A.B., and J.H. Van der Merwe. 1983. "The Growth of Dislocation-Free Layers." Chap. 27 in *Dislocations in Solids*, v. 6, ed. F.R.N. Nabarro. North-Holland.

Freund, L.B. 1992. "Dislocation Mechanisms of Relaxation in Strained Epitaxial Films." *MRS Bull.* July:52.

Herman, M.A., and H. Sitter. 1989. *Molecular Beam Epitaxy: Fundamentals and Current Status*. Berlin: Springer-Verlag.

Houng, Y.-M. 1992. "Chemical Beam Epitaxy." *Crit. Rev. in Solid State and Mater. Sci.* 17:277.

Hull, D., and D.J. Bacon. 1984. *Introduction to Dislocations*, 3rd ed. Oxford, U.K.: Pergamon Press.

Joyce, B.A. 1985. "Molecular Beam Epitaxy." *Rep. Prog. Phys.* 48:1637.

Saloner, D. 1986. "Characterization of Surface Defects and Determination of Overlayer Nucleation and Growth by Surface-Sensitive Diffraction." *Appl. Surf. Sci.* 26:418.

Suntola, T. 1989. "Atomic Layer Epitaxy." *Materials Science Reports* 4:261.

Tsao, J.Y. 1992. *Materials Fundamentals of Molecular Beam Epitaxy*. Boston, Mass.: Academic Press.

Weisbuch, C., and B. Vinter. 1991. *Quantum Semiconductor Structures*. Boston, Mass.: Academic Press.

Chapter

7

Chemical Vapor Deposition

The use of chemical vapors and gases as sources of film-forming elements was introduced in Sec. 6.5.4 in the context of epitaxy in the high-vacuum regime (Kn > 1). In this chapter, we consider the use of these sources at higher pressures in the fluid-flow regime (Kn << 1), where the process is known as chemical vapor deposition (CVD). Gaseous source materials allow process operation in this regime because they do not condense (by definition) on surrounding room-T surfaces during transport to the substrate. Therefore, the line-of-sight transport geometry from source to substrate which is required in the physical vapor-deposition (PVD) processes is not required in CVD. A monolayer or two of transporting gas may *adsorb* on the room-T surfaces, but this adsorption quickly saturates. On the other hand, upon reaching the heated substrate or other hot surfaces, some fraction of the adsorbing gas reacts to form the film. This fraction is expressed by the sticking coefficient, S_c, defined by Eq. (6.17). It is sometimes referred to as the "reactive" sticking coefficient, although this term seems redundant. Often, $S_c << 1$ at the substrate, and this makes it possible to uniformly coat substrates having convoluted surfaces, such as microcircuit patterns, or to coat large batches of substrates on all sides at once, such as tool bits. With $S_c << 1$, the gas can still reach remote substrate areas despite many encounters with hot surfaces along the way. This process was illustrated in contrast to PVD behavior for the filling of a trench in Fig. 5.17*f*.

The potential for uniform coating of nonplanar substrates—that is, "conformal" coating—is a key advantage of using gaseous sources in either flow regime of Kn. Various other advantages and disadvantages were mentioned in Sec. 6.5.4. Three additional advantages apply spe-

cifically to the higher-pressure regime. One is that higher deposition rates can sometimes be obtained while still maintaining conformality. Another is that simultaneous etching of the depositing film can often be achieved by establishing sufficient partial pressure of a suitable chemical etchant. This technique can improve selectivity when one wants to deposit only on activated surface areas, or only on one crystallographic plane (anisotropic epitaxy), or only one of the possible solid phases, as in diamond versus graphitic C. The third advantage of higher process pressure is that only one stage of pumping is required ("low-pressure" or LP-CVD), or no pumping in the case of atmospheric-pressure operation (AP-CVD). However, the gas-transport problems to be discussed below are all more difficult to deal with in APCVD than in LPCVD.

The basic thin-film process sequence of gas supply, transport, and deposition from Fig. 1.1 is presented in more detail for the case of CVD in Fig. 7.1. The gas-transport step is much more complex in the fluid-flow regime than in molecular flow, and therefore much of the chapter will be devoted to examining transport behaviors—mainly, free convection, homogeneous reaction, and diffusion. The discussion of the deposition step will focus on its surface processes, since most of what has previously been said about bulk film structure and interaction in Chaps. 5 and 6 also applies to CVD films. To give a flavor of the chemistry involved in CVD, Table 7.1 lists some of the commonly used *overall* reactions and their chemical types; many others are listed elsewhere [1,2]. We will see later that such overall reactions really consist of a series of reaction steps, some in the gas phase (homogeneous) and some on the surface (heterogeneous). Each reaction step has a rate determined by activation energy and process conditions, and any one of these rates can be the one that controls the film deposition rate. Alternatively, the gas-supply or transport step can be the one which controls deposition rate. Control by one or another of the steps in Fig. 7.1 has various advantages which will become clear below. It is important in CVD to determine the range of process conditions over which each step becomes the controlling one, and we will examine several techniques for doing so. The pyrolysis of silane (SiH_4) to deposit Si will often be used as an example, because it is one of the most extensively studied reactions. It is also quite complex, despite the simple overall reaction, so it illustrates all of the reaction phenomena to be discussed.

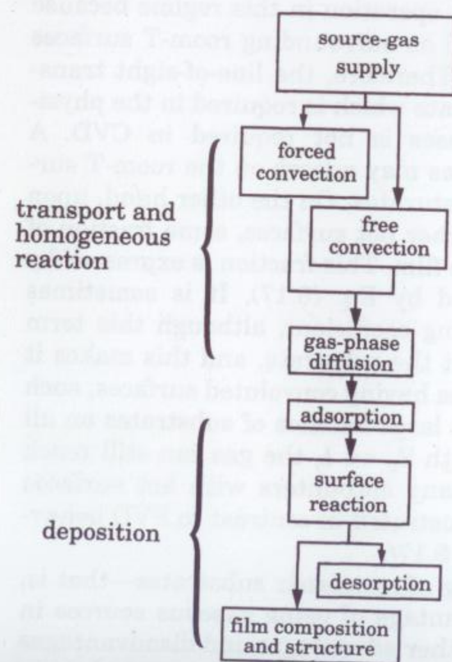

Figure 7.1 Sequence of process steps in CVD.

TABLE 7.1 Typical Overall Reactions Used in CVD

Type	Reaction
pyrolysis (thermal decomposition)	$SiH_4(g) \rightarrow Si(c) + 2H_2(g)$
	$SiH_2Cl_2(g) \rightarrow Si(c) + 2HCl(g)$
	$CH_4(g) \rightarrow C(\text{diamond or graphite}) + 2H_2(g)$
	$Ni(CO)_4(g) \rightarrow Ni(c) + 4CO(g)$
oxidation	$SiH_4(g) + 2O_2(g) \rightarrow SiO_2(c) + 2H_2O(g)$
	$3SiH_4(g) + 4NH_3(g) \rightarrow Si_3N_4(c) + 12H_2(g)$
hydrolysis	$2AlCl_3(g) + 3H_2O(g) \rightarrow Al_2O_3(c) + 6HCl(g)$
reduction	$WF_6(g) + 3H_2(g) \rightarrow W(c) + 6HF(g)$
displacement	$Ga(CH_3)_3(g) + AsH_3(g) \rightarrow GaAs(c) + 3CH_4(g)$
	$ZnCl_2(g) + H_2S(g) \rightarrow ZnS(c) + 2HCl(g)$
	$2TiCl_4(g) + 2NH_3(g) + H_2(g) \rightarrow TiN(c) + 8HCl(g)$

7.1 Gas Supply

Figure 7.2 illustrates typical elements of the "gas jungle" of plumbing used to supply CVD source gases and vapors to the deposition reactor. Not all of these elements will be used in a given reactor, and actual design will depend on the degree of gas hazard involved and on the operating pressures at the source and in the reactor. There are three aspects to gas-supply design: (1) protection of personnel and environ-

Figure 7.2 Typical elements of reactor gas-supply plumbing.

ment from the frequently hazardous properties of the reactants, (2) regulation of a steady and known flow of each gas, and (3) minimization of contamination in the process stream. We will discuss each of these aspects in turn below.

7.1.1 Safety

Gas-supply safety starts with careful design and construction to minimize the possibility of leaks or valve-operation errors. It also provides detection of hazardous conditions such as excess pressure or leaks before they become catastrophic, coupled with automatic shutdown of the gas supply. Leak prevention is also important for process purity. Plumbing should be welded wherever possible, and metal-gasketed connecting fittings should be used elsewhere. Fittings that seal directly against the tubing instead of against a welded-on flange are not recommended, because they develop leaks more easily when stressed. Valves should have bellows or diaphragm stem seals. Wherever elastomeric seals are unavoidable, the elastomer must be chemically compatible with the reactant gas.

Let us examine the safety elements in Fig. 7.2, following the gas flow path. The high-pressure gas cylinder (*a*) is stored in an outdoor cabinet connected to an exhaust duct, to minimize personnel exposure in the event of a leak. Gas sensors in the duct (*b*) as well as in the reactor-cabinet exhaust duct (*c*) and in the room (*d*) automatically shut off the pneumatically operated valves upon detecting a hazardous level. The first pneumatic valve is best installed *in* the gas cylinder at (*e*) if the gas supplier can do so. Otherwise, it can be mounted on a nearby panel at (*f*). The flow-restricting orifice (*g*) is mounted in the gas-cylinder valve by the supplier, and it limits the rate of gas discharge in the event of a break downstream. Discharge rate can be estimated as described in Appendix E. Further protection against a break is provided by the "excess-flow" valve (*h*), which slams shut when flow rate exceeds a certain level and stays shut until reset. The tubing loop (*i*) avoids stressing the plumbing when changing cylinders. The argon purge assembly (*j*) allows "rinsing" reactant gas out of the plumbing prior to cylinder change, using a series of pumpout/backfill cycles. It also minimizes intrusion of moisture during cylinder change. The argon supply must be separate for each gas so as to contain the gas in the event of backmixing. The outlet pressure gauge on the gas-pressure regulator incorporates an overpressure switch (*k*), which closes the pneumatic valve in the event of regulator failure. Regulator outlet pressure can creep up over time if the diaphragm's valve seat becomes contaminated or corroded. The final valve (*f*) isolates the gas cabinet when not in use.

Proceeding downstream from the gas cabinet, the supply line to the reactor (*m*) is double-contained to direct any leaking gas into the exhausted enclosures. Just after the flow-control assembly on this gas (*n-o-p*) as well as on the other two reactants are pneumatic valves (*q*) which provide hard shutoff in several instances: (1) when the gas is not being used, (2) when a leak is detected at any of the sensors, and (3) when excess downstream pressure is detected by the pressure switch at (*r*). This switch must be located upstream of the reactor's inlet shutoff valve (*s*) to prevent inadvertent backmixing of gases when (*s*) is closed. The gas plumbing, the low-pressure vapor sources (*t* and *u*), and the reactor are all contained in an exhausted cabinet. Downstream of the reactor, the gas-supply and bypass manifolds can be isolated from the pump and the gas exhaust system by valves (*v*) and (*w*), respectively. Pumping and exhaust treatment of hazardous gases was discussed in Sec. 3.2. Devices monitoring proper operation of the exhaust treatment system should shut the pneumatic valves (*e*) or (*f*) and also (*q*) in the event of malfunction.

The above discussion only illustrates some safety elements that might be desirable in a hazardous-gas supply system; it is not intended to represent a recommended system design. Actual design must follow local government and institutional codes. Hazards and recommended handling procedures for specific materials are described on the Material Safety Data Sheets (MSDSs) that the material's manufacturer is required to supply.

7.1.2 Flow control

The mass flow controller (*n-o*) is almost always the device used to regulate gas flow rate in CVD at any process pressure. It consists of a flow sensor (*n*) coupled to an electrically driven variable-leak valve (*o*) using a feedback loop similar to that used for T control in Sec. 4.5.3, so that it controls flow to a set point. Valve (*o*) does not provide reliable hard shutoff, so valve (*q*) is also needed. The mass flow controller is illustrated in more detail in Fig. 7.3. For high gas flows, the shunt path accommodates the excess gas to keep the sensor tube within its linear operating range of about 10 sccm. (See Sec. 2.5 for sccm definition.) Total flow range may be changed by substituting shunt orifices. In one typical sensor-tube design, a heater establishes a T profile along the tube which is symmetric at zero flow ($T_1 = T_2$). With flow, T_1 decreases and T_2 increases in proportion to the *thermal-mass* flow rate, where the thermal mass is the number of moles times the heat capacity per *mole* at constant *pressure*, c_p. (Section 2.4 discusses the various ways of expressing gas heat capacity; it is important to use the correct one.) The T imbalance occurs because heat is taken up by the gas, carried downstream, and deposited back onto the tube. Thus,

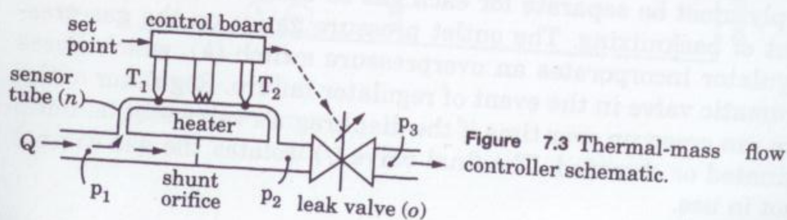

Figure 7.3 Thermal-mass flow controller schematic.

$$T_2 - T_1 = Bc_pQ \tag{7.1}$$

where B is a proportionality constant and Q is the "mass" (molar) flow rate in sccm. This relationship relies on the gaseous thermal conduction being fast radially and slow axially. In practice, deviations from this condition lead to slight nonlinearity [3].

Manufacturers do not calibrate flow controllers with hazardous gases; they proportion the calibration from that of a standard gas such as N_2 using known values of c_p. The Q of gas A which gives the same $(T_2 - T_1)$ signal as a flow $Q(N_2)$ of N_2 is found from Eq. (7.1) to be

$$Q(A) = \frac{c_p(N_2)}{c_p(A)}Q(N_2) = K_f Q(N_2) \tag{7.2}$$

where K_f is the calibration factor relative to N_2. Usually, c_p can be found in the literature. However, for accurate work it is best to calibrate the flow controller on the reactor by using the actual process gas and by spanning a range of flow rates to determine nonlinearity. This can be done easily using the gas leakup rate into a reactor closed off at the outlet. A calibrated pressure gauge such as the capacitance diaphragm gauge discussed in Sec. 3.5 is needed on the reactor, as shown at position (*x*) in Fig. 7.2. The enclosed volume, V_r, from the flow controller to the reactor's outlet valve (*v*) and including the supply manifold, must also be determined. This can be done by expansion of gas into the evacuated reactor from a flask of known volume V_0 at known pressure p_0 and use of the ideal-gas law, Eq. (2.10), whereby pV must be the same before and after the expansion. The mass flow rate is then found from the leakup rate and Eq. (2.10):

$$\frac{Q}{22{,}400} = \frac{dN_m}{dt} = \left(\frac{V_r}{RT}\right)\frac{dp}{dt} \tag{7.3}$$

where 22,400 is the molar volume, V_m (cm^3/mol), at 0° C and 1 atm, and t is in minutes for Q in sccm.

Mass flow controllers require $\approx 10^3$ Pa of pressure drop across the narrow sensor tube to drive the flow, so they are unsuitable for source vapors having very low vapor pressure, p_v. They are also unsuitable for handling vapors which decompose when moderately heated or are very reactive. In such cases, liquid-source flow-control systems [4] such as those shown at (*t*) or (*u*) in Fig. 7.2 can be used. In either case, the liquid container must be immersed in a constant-T enclosure held at somewhat below room T, to stabilize p_v and to prevent downstream condensation and resulting flow instability. Estimation of p_v was discussed in Sec. 4.1. In system (*t*), a suitable carrier gas such as H_2 or Ar bubbles through the liquid and carries the reactant vapor downstream. Carrier-gas flow rate needs to be very low so that vapor-liquid equilibrium can be sustained. Then, assuming ideal gas, the mole fraction of vapor in the stream is p_v/p_t, where p_t is the total pressure of the stream. In LPCVD or high-vacuum applications, p_t needs to be regulated by the feedback loop to leak valve (*y*). In APCVD applications requiring rapid switching of gas flow for multilayer film growth, flow toward the supply manifold may need to be increased by injecting additional carrier gas after valve (*q*) as shown. System (*u*) avoids the carrier gas but can be used only in LPCVD, because reactor pressure needs to be less than p_v to drive the flow. Flow is regulated by fixing leak valve (*z*) at a suitable conductance and then regulating the pressure upstream of it, p_z, using a pressure-control loop to leak valve (*y*). This system can be calibrated for Q versus p_z using the leakup method of Eq. (7.3). On the other hand, in system (*t*) only the carrier flow can be calibrated, and reactant-vapor flow estimation depends on knowledge of p_v.

Continuing downstream from the flow-regulating systems, pneumatically driven valves (*a′*) direct each flow stream into either the reactor supply manifold or the bypass manifold. This bypass is needed when rapid switching and restabilization of gas flow are required for multilayer films or atomic-layer epitaxy (Sec. 6.5.5). One cannot just valve off the flow at (*q*) or even at (*o*), because then pressure builds up to the upstream value (p_1 in Fig. 7.3) behind the valve and produces a flow burst when the valve is reopened. For the same reason, downstream pressure p_3 may need to be regulated using the gauge/valve control loops (*x*-*b′*) on the reactor outlet and (*c′*-*d′*) on the bypass manifold, with both manifolds held at the same pressure. Valve b′ is a motor-driven, butterfly-type throttle valve as was also shown in Fig. 3.1. In LPCVD, bypass-pressure regulation is not necessary because $p_3 << p_1$, but reactor-pressure regulation is still needed for deposition-process control. Pressure stability upstream of the mass flow controllers is also important, even though their calibration is nominally pressure-independent by Eq. (7.1). Slow pressure drift is tolerable, but an abrupt change in p_1 of Fig. 7.2 will cause a transient flow disturbance. For example, if p_1 drops by more than ($p_1 - p_2$), which is only $\approx 10^3$ Pa, there will actually be a temporary *backflow* through the sensor tube, which will cause the control loop to drive valve (o) wide open, resulting in a large flow burst. This transient disturbance is illustrated in Fig. 7.4. To avoid such disturbances when supply lines are shared among reactors, each mass flow controller should have its own pressure regulator.

7.1.3 Contamination

Impurities can occur in the gas or liquid as supplied by the manufacturer and can also intrude during vapor transport, just as in the case of solid source materials. Evolution ("outgassing") of impurities, especially water, from the internal surfaces of the gas-supply plumbing and control devices is a major source of contamination, and the comments of Sec. 3.4.2 on minimizing this problem in vacuum systems apply equally well here. The consequences of an impurity to the process of course depend on the film material and its application. For example, water *may* not be a serious contaminant in oxide deposition, but it is disastrous in (AlGa)As epitaxy.

The reactor must be cleaned before film deposition until the outgassing rate drops to an acceptable level. It is important to realize that this rate is not affected by the reactor operating pressure or by the ultimate vacuum level which the reactor pump can achieve. It is determined by surface conditions and is pressure-dependent only if the partial pressure of the outgassing species begins to approach its p_v, as discussed in Sec. 4.2. Thus, to avoid slowing down the cleanup rate, partial pressure should be kept low by flowing carrier gas. A long period of purging with carrier gas, or even better with a source vapor reactive with water, can clean up the plumbing just as well as can pumping to high vacuum. With sufficiently pure source materials and clean plumbing, it is possible to grow semiconductor-device-quality

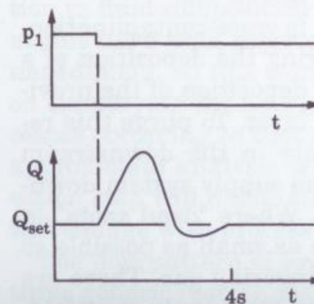

Figure 7.4 Transient flow response of a mass flow controller to a step change in upstream pressure, p_1.

epitaxial films in an APCVD reactor with no pumping at all. When it is desired to pump to high vacuum, such as for He leak checking, one must beware of contamination from backstreaming of pump oil (Sec. 3.4.1). When pumping out a gas supply line, the mass-flow-controller bypass valve (*p*) shown in Fig. 7.2 should be opened to increase conductance. Also note that no check valves are used in the supply plumbing, because these typically require a pressure drop of at least 0.1 atm to open. They therefore prevent both pumpout and leak checking. Backflow protection must be achieved in other ways, such as by the overpressure interlock (*r-q*). Despite the above procedures, there will always be some residual amount of outgassing load, Q_i. The partial pressure, p_i, of these contaminants in the reactor is minimized by using a large flow of carrier gas, Q_s, in accordance with Eq. (3.9).

Impurities coming from the source gases must be dealt with by the manufacturer. Here, the containing-cylinder material and its internal-surface preparation are as important as the chemical manufacturing process, especially with reactive gases. Carrier gases are available in very high purity, but final purification at the reactor may still be desired. For H_2, devices are available for diffusing it through hot Pd foil, which blocks all other gases. Inert gases such as Ar can be passed through "getters." These contain a reactive surface which chemisorbs reactive impurities. The Ti-sublimation type of getter can be reactivated periodically by sublimating a fresh layer of Ti. Water and O_2 can be removed by bubbling the carrier gas through Ga-In-Al alloy [5], which is liquid at room T and in which these impurities rapidly oxidize the Al. A "dew point" of $<-80°$ C is claimed for this process, the dew point being the T at which the p_v of water becomes less than its partial pressure in the gas mixture, so that dew condenses. Figure 4.4 shows that the p_v of water at $-80°$ C is 5×10^{-2} Pa, or 0.5 ppm in a 1 atm mixture. Purity of the process stream can be monitored to parts-per-billion (ppb) levels by two types of devices. Solid-state electrolytic sensors are available for specific gases such as H_2O and O_2. Mass spectrometers can detect all gases, and special ionization sources are available which operate at 1 atm, as discussed in Sec. 3.5.

The last source of impurities to be discussed is cross-contamination. When gas-stream composition is switched during the deposition of a multilayer film, gas remaining upstream from deposition of the previous layer becomes a contaminant for the next layer. To purge this remaining gas out quickly, sufficient gas velocity in the downstream direction must be maintained in all parts of the supply system downstream of the switching valves (*a′*) in Fig. 7.2. Where "dead spots" in the flow are unavoidable, they should be made as small as possible so that diffusion can more readily clear out the lingering gas. There are unavoidable dead spots between valves (*a′*) and the supply manifold, between the pressure switch (r) and the manifold, and between the pressure gauge (x) and the reactor. The reactor itself must be carefully designed to avoid dead spots, and this will be discussed in the next section.

7.2 Convection

Convection in a CVD reactor refers to the flow of the gaseous fluid as it moves through the reactor after being injected from the gas supply line. There is forced convection due a pressure gradient, and there can also be "free" convection due to the buoyancy of hot gas. On the other hand, when the gas gets very close to the substrate surface, flow velocity slows down due to viscous friction, and the remaining transport of reactant to the surface can only occur by *diffusion* through this relatively stationary "boundary" layer of fluid (see Fig. 7.1). Detailed knowledge of the flow pattern is needed to determine how far from the deposition surface this very important transition from convective to diffusive transport is occurring and which of these two transport steps is limiting reactant arrival rate at the surface. Convection is addressed in the subsections below, and diffusion will be addressed in Sec. 7.4. The flow pattern also determines gas residence time in the reactor and the extent of gas heating. Both of these factors influence the extent of homogeneous (gas-phase) reaction, an important aspect of CVD chemistry to be discussed in Sec. 7.3.

A complete description of fluid flow involves applying, to each point in the volume, the principles of mass, momentum, and energy conservation, along with the equation of state of the fluid. The equation of state relates pressure (p), T, and mass density (ρ_m); in CVD, the ideal-gas law, Eq. (2.10), is used. The resulting "Navier-Stokes" equations give the p, ρ_m, and velocity vector of the fluid at every point. A few analytical solutions for simple flow situations will be presented below. Some results from computer solutions of more complex flow patterns will also be presented. A full description of CVD requires adding to these equations the homogeneous reactions and the resulting variation in fluid composition through the reactor. Although some attempts at this have been reported, lack of reaction-rate data remains a major impediment, so this work will not be discussed. We will focus instead on simplifying the flow model and separately treating the various processes occurring so that simple calculations can be made. This kind of approximate analysis is easily done and is very useful in predicting which step will dominate a given CVD process and how the situation will change with process conditions.

The flow pattern of course depends on geometry, so we will consider three generic reactor designs in the following sections, as illustrated in

Fig. 7.5. There we show the substrates as flat wafers, but they may be any shape. Of the three reactors, the axisymmetric one delivers the reactant most uniformly to the substrate surface. The tube reactor has higher substrate capacity, but care must be taken to compensate for reactant depletion toward the downstream end. In these two reactors, one usually heats only the substrate region to minimize deposition elsewhere. This is conveniently done as shown in the figure, by inductively coupling radio-frequency (rf) power from the external coil to the conducting platform ("susceptor") on which the wafers lie. This arrangement is essentially a transformer which is generating a circulating current and joule (I^2R) heating in the susceptor. The third reactor is the batch type. It has the highest capacity, but there is *no* convective transport of reactant to the center surface areas of the substrates. To obtain deposition uniformity across these substrates, process conditions must be such that the reactant diffusion rate through the gap between the substrates is much faster than the deposition rate. That is, deposition rate must be limited by the reaction rate at the substrate surface. Since reaction rates increase exponentially with T [Eq. (5.16)], very good T uniformity must be established by immersing the entire reactor in a furnace. In the other reactors, the lower T uniformity obtainable with susceptor heating is acceptable as long as deposition rate is being limited *instead* by convection or diffusion.

7.2.1 Laminar flow in ducts

This simple fluid-flow model adequately describes many CVD situations. The mean fluid velocity, $\bar{u}$, needs to be low enough in CVD so that the gases will have time to diffuse to the substrate surface and react there before being swept out of the reactor. A typical value of $\bar{u}$

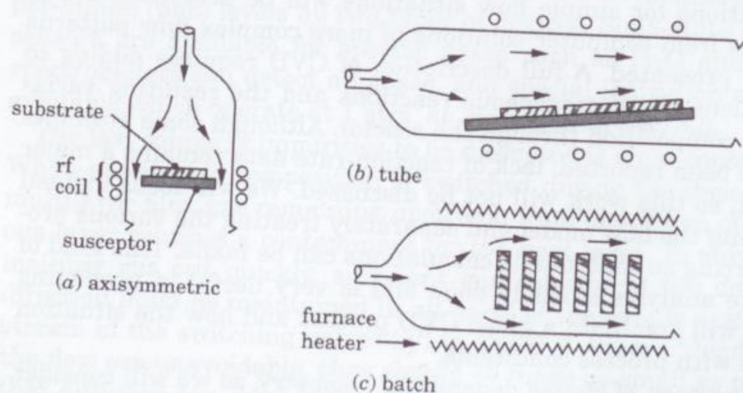

Figure 7.5 Generic reactor types.

is 4 cm/s whether the operating pressure is 10^5 Pa (1 atm) or 10^2 Pa (LPCVD). Consider a tube reactor of radius r_o = 5 cm. We can relate this u to the mass flow rate, Q (sccs), and to the volume flow rate, W (cm^3/s), using the ideal-gas law, Eq. (2.10):

$$Q = W\frac{22{,}400}{V_m} = \pi r_o^2 \bar{u}\,\frac{22{,}400}{RT/p} \qquad (7.4)$$

Thus, Q = 310 sccs = 19 slm at 1 atm, and Q = 0.3 sccs = 18 sccm at 10^2 Pa. Most of the Q consists of carrier gas at 1 atm and of reactant at 10^2 Pa, because the Q of reactant needs to be of the same order in both cases.

At such low $\bar{u}$, the flow pattern consists of smooth layers ("lamina") of fluid moving past each other under the constraint of viscous friction. At much higher $\bar{u}$, which is not encountered in CVD, these lamina break up and the flow becomes turbulent, which means that its velocity vector changes with position and time in a chaotic manner. Turbulent flow always reverts to laminar flow in a "boundary layer" adjacent to surfaces, due to viscous drag. There is no such boundary layer in CVD, because in laminar flow, u varies smoothly across the reactor. There are *other* boundary layers in CVD which we will discuss later.

Steady-state laminar flow in cylindrical tubes is a simple one-dimensional flow situation which applies to the axisymmetric and tube reactors. The radial velocity profile, u(r), can be obtained by a force balance between pressure drop and viscous shear along the unit-length cylindrical section shown in Fig. 7.6:

$$\pi r^2 \Delta p = 2\pi r \tau = 2\pi r \eta \frac{du}{dr} \qquad (7.5)$$

Here, Eq. (2.28) relating shear stress, τ, to viscosity, η, has been used to obtain the second equality. This equation is integrated with the

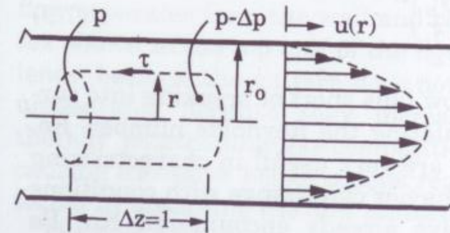

Figure 7.6 Force balance and flow-velocity profile, u(r), for steady-state laminar flow in a cylindrical tube of radius r_o.

boundary condition that u = 0 at the wall ($r = r_o$), which is valid for Kn << 1. We then arrive at the classic parabolic velocity profile of "Poiseuille" flow,

$$u(r) = \frac{\Delta p}{4\eta}\left(r_o^2 - r^2\right) \tag{7.6}$$

as shown on the right-hand side of Fig. 7.6. The mean value of u is found by integrating over the cross section:

$$\bar{u} = \frac{\int_0^{r_o} u\,(2\pi r)\,dr}{\pi r_o^2} = \left(\frac{\Delta p}{8\eta}\right) r_o^2 \tag{7.7}$$

For the $\bar{u}$ and r_o used above and for $\eta = 88\ \mu P = 8.8\times10^{-6}$ Pa·s (H_2 at room T), we find that $\Delta p = 10^{-5}$ Pa/cm, a negligible value even in LPCVD. Thus, we can *neglect* total pressure variations in analyzing CVD-reactor processes, except in the special case of the thermal-transpiration pressure drop into a pressure gauge connected by a narrow tube in which Kn > 1 [Eq. (3.18)].

A parabolic u profile is also obtained for flow between parallel plates (Exercise 7.2). This situation would apply to a rectangular-tube reactor of large width/height ratio. For a height of y_o and for y = 0 at the centerline,

$$u(y) = \frac{\Delta p}{2\eta}\left(\frac{y_o^2}{4} - y^2\right) \tag{7.8}$$

and

$$\bar{u} = \left(\frac{\Delta p}{3\eta}\right)\left(\frac{y_o}{2}\right)^2 \tag{7.9}$$

The degree to which the reactor flow falls short of breaking into turbulence can be determined by calculating the Reynolds number, Re. Dimensionless numbers such as Re are very useful in characterizing transport situations in which the behavior can change with conditions from one mode to another. We have already encountered Kn, Pe [Eq. (6.23)], and the deposition purity ratio (Sec. 2.6). The importance of Re warrants a brief derivation here. Re is the ratio of the momentum (inertial) force to the viscous-drag force operating on the fluid. These forces respectively destabilize and stabilize the flow pattern,

and when Re exceeds 1200 or so depending on geometry, turbulent instability begins. For flow in a tube, the momentum per length z of tube is $\mathbf{k} = (\pi r_o^2 z)\rho_m \bar{u}$, where ρ_m is the fluid's mass density. The force that would be required to stop this momentum within length z is $\mathbf{k}(du/dz) = \mathbf{k}\bar{u}/z = \pi r_o^2 \rho_m \bar{u}^2$. The viscous drag force on the fluid against the wall is $(2\pi r_o z)\eta|du/dr|$, where |du/dr| is evaluated at r_o using Eqs. (7.5) and (7.7): $|du/dr| = 4\bar{u}/r_o$. Taking the ratio of these two forces and dropping the numerical factors, we have

$$Re = \frac{r_o^2 \rho_m \bar{u}}{z\eta} = \frac{L\bar{u}}{(\eta/\rho_m)} = \frac{L\bar{u}}{\nu} = \frac{L\bar{u}}{\eta}\left(\frac{pM}{RT}\right) \tag{7.10}$$

where (r_o^2/z) has been replaced by L to represent a characteristic linear dimension of the reactor for the more general case. The "kinematic" viscosity, ν (cm^2/s, or Stokes) = η/ρ_m, may be thought of as the "momentum diffusivity" and is analogous to the mass diffusivity, D (cm^2/s). The last equality in Eq. (7.10) assumes ideal gas and shows that Re decreases with decreasing p at a given $\bar{u}$, since η is independent of p by Eq. (2.28). Using $\eta = 88\ \mu P = 8.8\times10^{-5}$ g/cm·s and $\rho_m = 8.2\times10^{-5}$ g/cm^3 for H_2 at room T and 1 atm, so that $\nu = 1.07$ cm^2/s, and using L = 5 cm and $\bar{u}$ = 4 cm/s, we see that the units cancel in Eq. (7.10) as they should, and that Re = 19. This is way below the onset of turbulence, and it would be even lower at lower p, so we conclude that *flow is always laminar* in CVD.

More complicated flow patterns than the parabolic one are often encountered, however. These can be caused by abrupt changes in flow path or by steep T gradients. We will consider T gradients in Sec. 7.2.3. The flow path changes first at the point of gas injection, where the supply line expands to the reactor diameter. If the expansion is gradual and u is not too high, one obtains the nearly parallel flow pattern shown in the bottom half of Fig. 7.7. However, if the expansion is too rapid, because of an abrupt diameter change or excessive u, the flow separates from the wall and recirculates in the "Hamel-flow" vortex shown in the top half of the figure [6]. Note that this is not turbulence, because the pattern does not vary with time. Such vortices are undesirable because they increase the reactant residence time, thereby lengthening gas-composition switching time and sometimes causing excessive homogeneous reaction. Their occurrence can be detected by observing the flow patterns using tracer smoke.

The flow path changes next upon encountering the susceptor, where u must drop to zero due to viscous drag along this new surface, as shown in Fig. 7.8 for the tube reactor geometry. But within only a few L lengths downstream at the low Re of CVD, the parabolic profile is re-

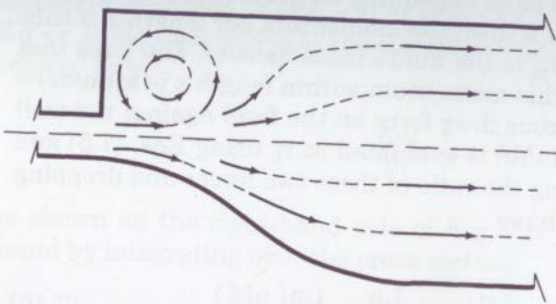

Figure 7.7 Two alternative reactor-entrance geometries and flow patterns (upper and lower halves). The upper pattern is to be avoided.

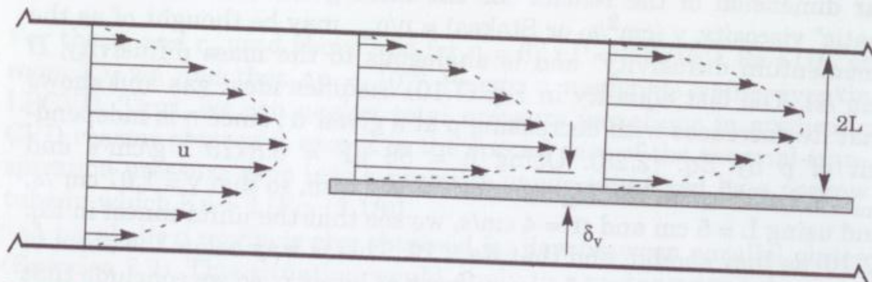

Figure 7.8 Velocity boundary layer of width δ_v forms at the susceptor leading edge in a tube reactor.

stored. The initial distortion of the profile does not affect the deposition rate significantly anyway, as we will see in Sec. 7.4. This flow situation is sometimes modeled with the susceptor acting as a wing passing through a stationary fluid at velocity –u. In the wing model, the position above the wing surface at which the fluid has become accelerated by 1 percent of the way toward –u is defined as the edge of the velocity boundary layer, δ_v. Clearly, δ_v will expand moving downstream along the wing, but for most of the length of a typical susceptor in a CVD tube, the u profile is parabolic and does not fit this model, so the concept of δ_v has no meaning. We will see below that there *is* a meaningful δ_v in the axisymmetric flow pattern.

7.2.2 Axisymmetric flow

In this reactor geometry (Fig. 7.5*a*), the flow pattern is similar to one of the few two-dimensional flow situations for which an analytical solution to the Navier-Stokes equations has been found. This solution is often used in modeling CVD, but we will see below that its applica-

bility is limited. The analytical solution [7] assumes that a stream of fluid of radius r_s is approaching an infinite, planar, stationary surface at uniform velocity u_z^∞ in the –z direction, as shown on the left-hand half of Fig. 7.9. At some point of approach, u_z begins to slow down, reaching a stagnation point of zero flow at z = 0 and r = 0. Meanwhile, radial velocity, u_r, begins to increase as the fluid becomes deflected by the surface. In the "potential-flow" region, far enough above the surface so that u_r is not slowed down by viscous drag against it, the functional forms

$$u_z = -2Bz \tag{7.11}$$

and

$$u_r = Br \tag{7.12}$$

are found to provide a solution [7] to the flow equations. Here, B is an unspecified constant. In this potential-flow region, the flow direction is changing while u_z remains independent of r and u_r remains independent of z, as shown in the figure. Closer to the surface, however, viscous drag causes u_r to decrease toward zero at z = 0, as also shown. The velocity boundary layer's edge is defined as before: it is the z value at which u_r is reduced by 1 percent from its free-stream value. With this

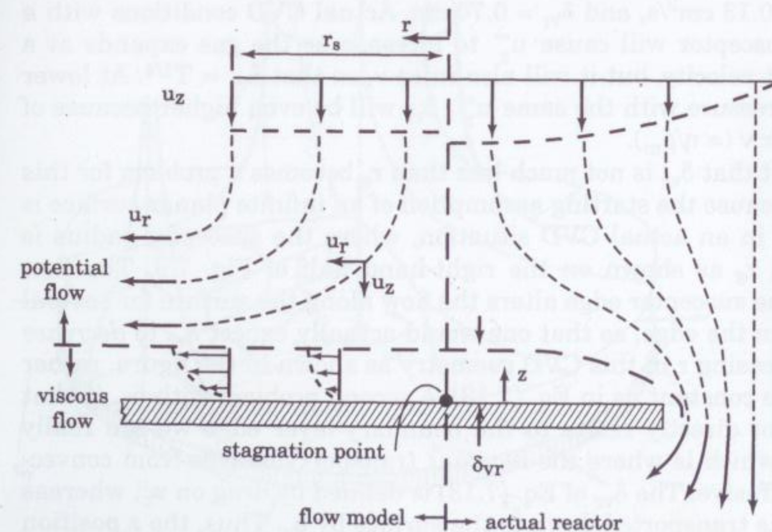

Figure 7.9 Axisymmetric flow geometry and approximate flow patterns for analytical flow model and for actual reactor.

definition and Eqs. (7.11) and (7.12), the thickness of the radial-velocity boundary layer is found to be

$$\delta_{vr} \approx 2.2\sqrt{\frac{\nu}{B}} \quad (7.13)$$

where ν is the kinematic viscosity [Eq. (7.10)]. Note that, according to this model, δ_{vr} is independent of r—at least for $r < r_s$. This is because two effects are cancelling each other: the increase in δ_{vr} with increasing downstream distance, r, as in Fig. 7.8, and the decrease in δ_{vr} due to the increase of u_r with r.

To estimate δ_{vr}, we need to determine B. Since for $r \geq r_s$, all of the flow has been redirected radially, it is reasonable to assume that $u_r \to u_r^\infty$ at $r = r_s$. Since kinetic energy is conserved in the potential-flow region, we also have $u_r^\infty = u_z^\infty$. Using this information in Eq. (7.12), we obtain $B = u_z^\infty / r_s$, so that

$$\delta_{vr} \approx 2.2\sqrt{\frac{\nu r_s}{u_z^\infty}} \quad (7.14)$$

Taking ν = 1.07 for H_2 at room T and 1 atm and $u_z^\infty = 4$ cm/s as in the last section, and using $r_s = 3$ cm, we find that $\delta_{vr} = 2.0$ cm—a value almost as big as r_s itself. Even for the much higher-density gas Ar, we have ν = 0.13 cm²/s, and $\delta_{vr} = 0.70$ cm. Actual CVD conditions with a heated susceptor will cause u_z^∞ to increase as the gas expands at a fixed inlet velocity, but it will also raise ν, so that $\delta_{vr} \propto T^{1/4}$. At lower reactor pressure with the same u_z^∞, δ_{vr} will be even higher because of the higher ν (= η/ρ_m).

The fact that δ_{vr} is not much less than r_s becomes a problem for this model, because the starting assumption of an infinite planar surface is not valid in an actual CVD situation, where the susceptor radius is less than r_s as shown on the right-hand half of Fig. 7.9. The flow around the susceptor edge alters the flow along the surface for several δ_{vr} in from the edge, so that one would actually expect δ_{vr} to *decrease* with increasing r in this CVD geometry as shown in the figure, rather than to be constant as in Eq. (7.13). A second problem with δ_{vr} is that it does not directly relate to the boundary-layer edge we are really seeking, which is where the *reactant* transport changes from convective to diffusive. The δ_{vr} of Eq. (7.13) is defined by drag on u_r, whereas reactant is transported down to the surface by u_z. Thus, the z position at which u_z starts to decrease could define the edge of another velocity boundary layer, δ_{vz}. From Eq. (7.11) and our estimate of B, we obtain simply

$$\delta_{vz} = r_s/2 \quad (7.15)$$

This, too, must be considered an oversimplification on account of edge effects, but again we see that δ_{vz} is not much less than r_s. Two main conclusions result from the above analysis of axisymmetric CVD flow with a stationary susceptor. First, the velocity boundary layers are never going to be much smaller than the susceptor radius under any reasonable flow conditions. Second, one must be careful (in any flow geometry) to select the appropriate boundary layer—the one that relates to *reactant* transport.

Rotating the susceptor disc at an angular velocity ω (rad/s) improves the above situation somewhat. The resulting flow pattern, shown in Fig. 7.10, is characterized by a boundary layer of fluid being dragged around with the disc and thrown outward by centrifugal force. This centrifugal-pumping action also sucks fluid down toward the disc along *z*. Thus, there are three velocity components: radial (u_r), circumferential (u_ω), and axial (u_z). Like the stationary disc, this special flow situation has an analytical solution [7, 8], given a disc radius much

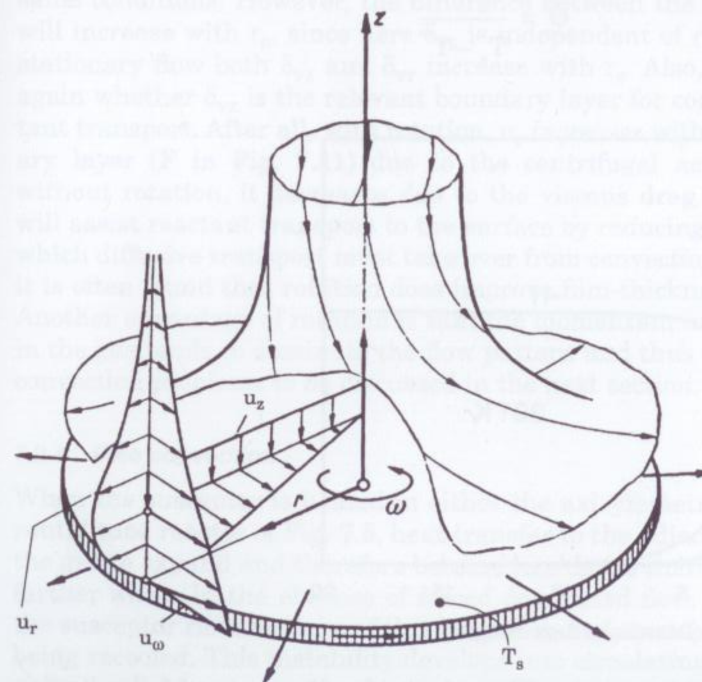

Figure 7.10 Axisymmetric flow pattern over a rotating disc. (Source: Reprinted from Ref. 7 by permission, © 1968 by McGraw-Hill Book Co.)

larger than δ_v and given no *externally* imposed u_z. Figure 7.11 shows the calculated behavior of the three velocity components versus z, all expressed in terms of the following dimensionless variables for height (ζ) and the velocities (F, G, H):

$$\zeta = z\sqrt{\frac{\omega}{\nu}} \tag{7.16}$$

$$u_r = r\omega F(\zeta) \tag{7.17}$$

$$u_\omega = r\omega G(\zeta) \tag{7.18}$$

$$u_z = \sqrt{\nu\omega}\, H(\zeta) \tag{7.19}$$

Also shown in Fig. 7.11 is the dimensionless T profile obtained when the susceptor is heated:

$$\Theta = \frac{T_z - T^\infty}{T_s - T^\infty}$$

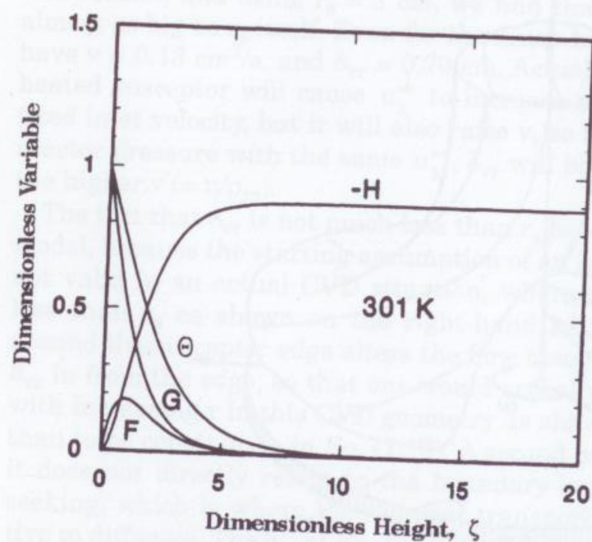

Figure 7.11 Profiles of dimensionless T (Θ) and velocity over the heated rotating disc shown in Fig. 7.10. The velocity components are radial (F), circumferential (G), and axial (H). (Source: Reprinted from Ref. 8 by permission.)

An asymptotic value of H = 0.884 for axial velocity is reached at a large height above the disc, so the corresponding u_z from Eq. (7.19) must be adjusted, by way of ω, to *match* the inlet flow velocity in the reactor tube, u_z^∞, if the calculated flow pattern is to be realized in an actual CVD reactor [8]. If ω is too low, the beneficial effect of the rotation in reducing δ_v will be lessened. If ω is too high, the excess flow being pumped will recirculate up the sidewall of the tube, producing an undesirable vortex similar to the one shown in Fig. 7.7. The onset of this flow disturbance has been observed using tracer smoke [8]. Taking $\nu = 1.07$ for H_2 at room T and 1 atm and $u_z^\infty = 4$ cm/s as before, we find that the upper limit to ω is 19 rad/s or 180 rpm. Given this, we can now determine δ_{vz} by observing in Fig. 7.11 that H has dropped by 1 percent at about $\zeta = 5$. Combining this with Eqs. (7.16) and (7.19) to eliminate ω, we have

$$\delta_{vz} \approx 4.4\nu/u_z^\infty \tag{7.20}$$

and for the above case of H_2 at 4 cm/s, $\delta_{vz} = 1.2$ cm. This is not much smaller than the δ_{vr} or δ_{vz} found for the stationary disc under the same conditions. However, the difference between the two δ_{vz} values will increase with r_s, since here δ_{vz} is independent of r_s; whereas, for stationary flow both δ_{vz} and δ_{vr} increase with r_s. Also, one must ask again whether δ_{vz} is the relevant boundary layer for considering reactant transport. After all, with rotation, u_r *increases* within that boundary layer (F in Fig. 7.11) due to the centrifugal action; whereas, without rotation, it decreases due to the viscous drag. This increase will assist reactant transport to the surface by reducing the z value at which diffusive transport must take over from convection. Empirically, it is often found that rotation does improve film-thickness uniformity. Another advantage of rotation is that the momentum induced thereby in the gas tends to dominate the flow pattern and thus avoid the free-convection problems to be discussed in the next section.

7.2.3 Free convection

When the susceptor is heated in either the axisymmetric or the horizontal tube reactor of Fig. 7.5, heat transfer to the adjacent gas causes the gas to expand and therefore become less dense than the cooler gas farther away. In the absence of forced downward flow, the gas above the susceptor rises because of this buoyancy, and then falls again after being recooled. This instability develops into circulating flow patterns or "roll cells" known as "free" or "natural" convection. Free convection will not develop in the isothermal batch reactor. Calculated circulation patterns (Jensen, 1989) for a horizontal tube reactor of rectangular

cross section are shown in Fig. 7.12*a*, looking along the z-axis direction of forced convection through the tube. The direction of circulation depends on the T of the tube sidewalls. For a tube with cooled sidewalls, the flow is downward near the sidewalls and upward near the centerline; whereas, with insulated sidewalls, the pattern is reversed. The direction and velocity of this flow affect the transport rate of reactant to the substrate and therefore affect the lateral uniformity profile of the deposited film.

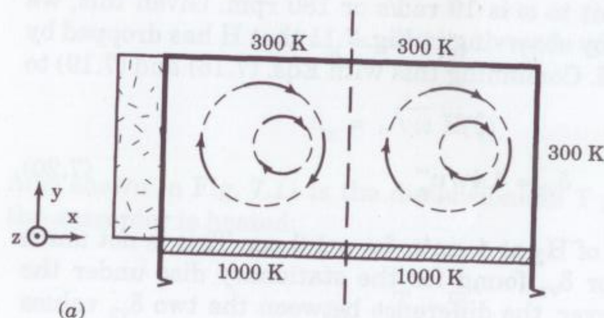

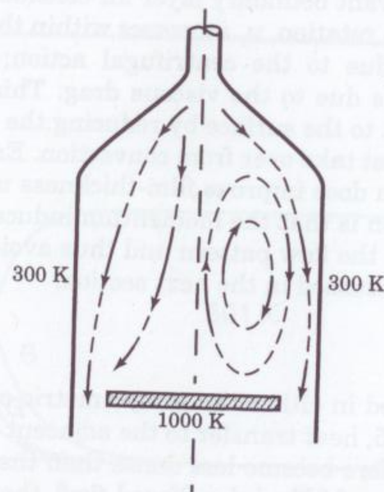

Figure 7.12 Typical free-convection roll cells: (*a*) horizontal rectangular-tube reactor (view along axis) with two alternate sidewall conditions, insulated (left) and cooled (right); (*b*) downflow axisymmetric reactor, showing two alternate flow patterns. In (*b*), the recirculating pattern (right) is to be avoided.

The degree of free-convective flow scales with the ratio of buoyancy force to viscous force and with Re. These ratios together constitute the dimensionless Grashof number [9],

$$\mathrm{Gr} = \frac{\mathrm{Ra}}{\mathrm{Pr}} = \frac{\rho_m^2 g \alpha_{TV}\left(T_s - T^\infty\right)L^3}{\eta^2} = \frac{g\alpha_{TV}\left(T_s - T^\infty\right)L^3}{\nu^2}$$

$$= \frac{gM^2 p^2\left(T_s - T^\infty\right)L^3}{R^2 T^3 \eta^2} \tag{7.21}$$

where g = gravitational acceleration = 980 cm/s^2

$\alpha_{TV} = dV/VdT$ = volumetric thermal-expansion coefficient, K^{-1}

T_s = substrate or susceptor T, K

T = mean T of circulating gas, K

Other notation is as used above. The last equality assumes the ideal-gas law, Eq. (2.10). Sometimes the Rayleigh number, Ra, is used instead of Gr to evaluate free convection. For gases, Ra ≈ Gr, because the Prandtl number, Pr, is near unity.

$$\mathrm{Pr} = \frac{c_p}{M}\frac{\eta}{K_T} \approx 0.8 \pm 0.2$$

where c_p/M is the heat capacity per gram and K_T is the thermal conductivity. The characteristic dimension, L in Eq. (7.21), is taken as the smaller of the two dimensions in which the roll cell lies. Using $\nu = 1.07$ for 1 atm H_2, and taking L = 5 cm, we have Gr = 1.2×10^5—high enough that free convection definitely will occur.

The critical value of Gr above which free convection becomes significant cannot be stated quantitatively, because it varies with geometry and with the amount of forced convection. For example, Fig. 7.12*b* shows two alternate flow patterns in an axisymmetric reactor (Jensen, 1989). In the absence of forced downward flow, u_z, the circulation pattern shown at the right typically develops for large Gr. However, there is always a finite u_z in CVD, and a large enough u_z will eliminate the circulation, producing the more parallel flow shown on the left of the figure. In addition, the flow pattern is *bistable* over some range of Gr and u_z. That is, if the circulation pattern is allowed to develop before the u_z flow is turned on, it can persist to larger u_z than if flow is started before the susceptor is heated. Reactor shape and susceptor rotation will also affect the critical value of Gr.

Circulation against the direction of u_z results in an undesirably long gas residence time in the reactor. Circulation transverse to u_z, as in Fig. 7.12*a*, can degrade uniformity. Inspection of Eq. (7.21) shows that reducing pressure is the most effective way of reducing Gr, since pressure is the most widely adjustable among the choices of process variables there. Low Gr is one of the main advantages of LPCVD over APCVD. In the case of the axisymmetric reactor, one can also just invert it so that the hotter gas is already at the top and there is no driving force for recirculation. However, this remedy requires supporting the substrate on its front face in a way which neither disturbs the flow pattern nor contaminates the growth surface.

Because of the difficulty of predicting flow patterns, it is best to examine them experimentally for the particular reactor at hand. This can be done easily using tracer smoke, but there are two problems. One is that smoke contaminates the reactor. The other is that in steep T gradients, the smoke patterns will be distorted from the actual flow pattern by the thermophoretic motion of particles down the T gradient, as will be discussed in Sec. 7.4.3. Alternatively, "schlieren" photography or interference holography [10] can be used to observe the patterns of optical interference fringes which result from refractive-index variation along the T gradient.

7.3 Reaction

The source gases become heated at some point during their transport to the substrate, this point depending on the type of reactor (Fig. 7.5) and the flow pattern within it. Thus, reaction often begins in the gas phase rather than occurring entirely on the substrate surface. The products of these reactions are usually more reactive with the substrate than are the source gases themselves. Excessive gas-phase reaction can produce particles of film material within the gas phase, and these settle out as powder. It is important in CVD to understand and control both the gas-phase and the surface reactions.

7.3.1 Chemical equilibrium

The simplest analysis of a reacting system assumes that all species reach chemical equilibrium with each other. Since CVD reactors are continuously producing a net change of reactant to product, they cannot be operating at equilibrium, which by definition entails no net change. Moreover, it is often necessary to operate *far* from equilibrium in order to avoid powder formation or to achieve deposition-rate uniformity over large areas, because these objectives are accomplished by flowing gas through the reactor much faster than it can react. Nevertheless, the calculation of equilibrium composition is a convenient and useful starting point for the analysis of a CVD process. At least it tells us what reactions are possible and how far they can proceed in the equilibrium *limit*. How far they actually proceed is determined by reaction rate and by gas-phase diffusion, which we will discuss later.

It was shown in Eqs. (4.4) through (4.6) that a reacting "system" operating at constant pressure, p, reaches equilibrium when its total Gibbs free energy, G, is minimized. [A system operating instead at constant V would reach equilibrium when the Helmholtz free energy, (G – pV), was minimized, but CVD always operates at constant p.] Here, G is in units of kJ for the total system, not in kJ/mol. The "system" under consideration starts as some fixed number of moles of the feed gas (supply gas) mixture, which then reacts to various gaseous and solid products as it moves through the reactor at constant p. For this mixture of reactant and product species, the total free energy is

$$G\,(\mathrm{kJ}) = \sum_i N_{mi}\mu_i \tag{7.22}$$

where N_{mi} is the number of moles of the ith species, and μ_i is its chemical potential. Recall from Eq. (4.7) that μ_i (kJ/mol) is the incremental Gibbs free energy per mole of i added to the mixture. We repeat here Eq. (5.28) for μ, which was derived for ideal gases.

$$\mu_i = \mu_i^\circ(T) + RT\ln\frac{p_i}{p^\circ} \tag{7.23}$$

This gives μ_i versus the partial pressure of i, p_i, in the reactor at temperature T, relative to $\mu_i^\circ(T)$, which is the μ_i at the standard reference pressure, $p^\circ = 10^5$ Pa ≈ 1 atm, and at the same T. Since the μ_i of an ideal gas at a given p_i is not influenced by the presence of other species, $\mu_i^\circ(T)$ is identical to the molar free energy of formation of that species from its elements in their standard states, $\Delta_f G_i^\circ$ (kJ/mol). The standard state of an element is its common phase (solid, liquid, or gas) at 10^5 Pa and 298 K, and that phase is assigned G = 0 at 10^5 Pa and *all* T. Most $\Delta_f G^\circ$ values can be found in handbooks [11,12] or in various on-line data bases [13]. Note that $\Delta_f G^\circ$ tends to be a slowly varying and often linear function of T; some examples are shown in Fig. 7.13.

For a gas-phase species, μ_i can be found from $\Delta_f G^\circ$ and p_i using Eq. (7.23). For condensed phases such as the depositing film, the p dependence of μ is negligible. When the film is a solid solution (an alloy) rather than a pure element or compound, the μ of each species in the solution is reduced by the mole fraction x_i to which it is diluted. For "ideal" solutions,

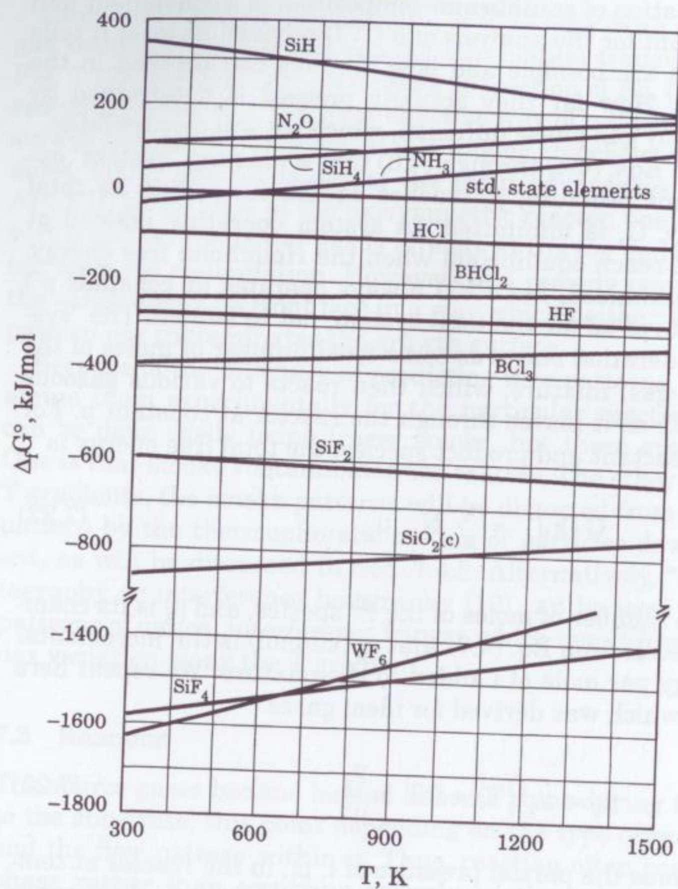

Figure 7.13 Gibbs free energies of formation for selected gaseous and solid (c) compounds at 10^5 Pa [12].

$$\mu_i = \mu_i°(T) + RT \ln x_i \qquad (7.24)$$

This dilution effect is closely related to the reduction of a species' vapor pressure by dilution [Eq. (4.21)]. However, for the present, we will deal only with pure solid phases.

Once the μ_i equations for the species in a reacting system have been written, the system's equilibrium composition can be determined numerically by minimizing system G in Eq. (7.22), subject to the following constraints: non-negative N_m values, fixed total p $(= \Sigma p_i)$, and conservation of the total amount of each element as it becomes distributed among the various product species (that is, conservation of mass). Programs such as SOLGASMIX [14] and BELLTHERM [15]

are available for calculating the thermodynamics of complex systems that are undergoing multiple simultaneous reactions. However, to obtain more insight into equilibrium behavior, we consider instead a single generalized reaction between molecules A and B to form products C and D:

$$\nu_A A + \nu_B B \leftrightarrows \nu_C C + \nu_D D \qquad (7.25)$$

Here, the ν_i values are the stoichiometric coefficients that satisfy the mass balance for all chemical elements in the reaction. The double arrow indicates that the reaction is reversible and proceeds in both directions. Some typical deposition (heterogeneous) reactions were listed in Table 7.1. Gas-phase (homogeneous) reactions can also be important, such as $SiH_4 \leftrightarrows SiH_2 + H_2$ and $BCl_3 + H_2 \leftrightarrows HBCl_2 + HCl$. (Note that all the ν_i values happen to be unity in these two reactions.) Assume for now that Eq. (7.25) is the only significant reaction of A and B, that some fraction, ξ, of A has reacted away, and that there is present an excess fraction, y, of B above the stoichiometric amount ν_B. Then, for ν_A moles of A at the start of reaction, Eq. (7.22) becomes

$$G = (1 - \xi)\nu_A\mu_A + (1 - \xi + y)\nu_B\mu_B + \xi(\nu_C\mu_C + \nu_D\mu_D) \qquad (7.26)$$

and at equilibrium,

$$dG/d\xi = 0 = -\nu_A\mu_A - \nu_B\mu_B + \nu_C\mu_C + \nu_D\mu_D \qquad (7.27)$$

where both ξ and y have vanished. Inserting Eq. (7.23) for μ_i gives

$$-\Delta_r G°(T) = -(\nu_C\mu_C° + \nu_D\mu_D° - \nu_A\mu_A° - \nu_B\mu_B°) = RT \ln \frac{(p^{\nu})_C (p^{\nu})_D}{(p^{\nu})_A (p^{\nu})_B (p°)^{\Delta\nu}} = RT \ln K \qquad (7.28)$$

where $\Delta_r G°$ is the free energy of reaction calculated from $\mu°$ data at the T of interest, and K is known as the equilibrium constant of the reaction. The net change in molarity, $\Delta\nu = \nu_C + \nu_D - \nu_A - \nu_B$, drops out of Eq. (7.28) if the p_i values are given in units of 10^5 Pa (≈ atm), since then the reference pressure p° = 1.

Equation (7.28) is the general form of the expression arrived at in Eq. (5.31), which applied to the first-order reaction of an adsorbed spe-

cies into a transition state. It is the central equation of chemical equilibrium. If there are multiple simultaneous reactions occurring, their equilibria must all be satisfied simultaneously, again subject to the constraint that $p = \Sigma p_i$. This p_i sum includes nonreacting species as well, so the result will vary with dilution if $\Delta\nu \neq 0$ (see Exercise 7.8). The mass-balance constraint in Eq. (7.28) is contained in the ν_i values, since they come from the balanced Eq. (7.25). Further discussion of equilibrium calculations is given by Smith (1980). Equation (7.28) can provide various types of information useful in CVD. It predicts the upper limit of reactant conversion to gaseous products (Exercises 7.7 and 7.8). It also tells whether deposition can occur and what solid phases are likely to form, and we give several examples of such prediction in the remainder of this section.

In integrated-circuit fabrication, the deposition of W from WF_6 vapor is sometimes used for Si contact metallization. Usually, selective deposition is desired, meaning deposition on the exposed Si areas but not on the surrounding SiO_2. The following reaction is the most favorable one on SiO_2; that is, it has the lowest $\Delta_rG°$:

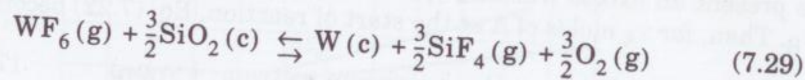

$$WF_6(g) + \tfrac{3}{2}SiO_2(c) \leftrightarrows W(c) + \tfrac{3}{2}SiF_4(g) + \tfrac{3}{2}O_2(g) \qquad (7.29)$$

where (g) and (c) denote gaseous and condensed (liquid or solid) phases. From the data of Fig. 7.13, it is found that at a typical deposition T of 700 K, $\Delta_rG° = +420$ kJ/mol for this reaction. Thus, using Eq. (7.28) with p_i in atm,

$$K = \frac{p^{3/2}(SiF_4)\,p^{3/2}(O_2)}{p(WF_6)} = \frac{p^3(SiF_4)}{p(WF_6)} = e^{-\Delta_rG°/RT}$$

$$= 10^{-420/2.3 \times 0.0083 \times 700} \approx 10^{-31} \qquad (7.30)$$

Note that there are no p_i terms here for the condensed-phase species, in accordance with the discussion following Eq. (7.23). The above result says that even for a high WF_6 p_i of 1 atm, the product-species p_i values would have to kept below 10^{-10} atm for the W deposition reaction to reach equilibrium. For higher product p_i values, the driving force toward equilibrium is in the reverse direction, that is, etching of W in an attempt to increase the p_i of WF_6. Since keeping the product p_i values this low would require a ridiculously high flow rate of WF_6, W cannot be deposited on SiO_2 from WF_6 alone. On the other hand, the reaction of WF_6 with *elemental* Si to form W and SiF_4 has a much lower $\Delta_rG°$ of −707 kJ/mol at 700 K, and in fact this reaction occurs readily up to a limiting W thickness of ≈ 20 nm which is imposed by the need for Si to diffuse through the W film [16]. Thicker W films are deposited using the reaction

$$WF_6 + 3H_2 \leftrightarrows W(c) + 6HF(g) \qquad (7.31)$$

or the reaction of WF_6 with SiH_4 gas to form W, HF, and SiF_4. Both of these reactions can be found from the data of Fig. 7.13 to be very favorable (large negative $\Delta_rG°$).

Manipulation of the p_i values which make up K can be used to drive a reaction in the desired direction. For example, C contamination in GaAs deposited from $(CH_3)_3Ga$ occurs due to CH_3 decomposition on the surface at high substrate T. Without knowing the details of the surface reaction mechanisms, one can assume an overall reaction, $C(a) + 2H_2(g) \leftrightarrows CH_4(g)$, which will be driven to the right by increasing $p(H_2)$. Indeed, the C level is found to be much lower using CVD in 1 atm of H_2 carrier gas than using chemical-beam epitaxy under vacuum (see Sec. 6.5.4).

In some depositions, more than one solid phase is possible, and then thermodynamics can be used to predict the favored phase. Thus, in depositing GaAs, liquid Ga may also be formed if one is not careful. In the GaAs-CVD T range around 1100 K, the principal volatile species produced in the decomposition of GaAs is As_2; thus, we can write

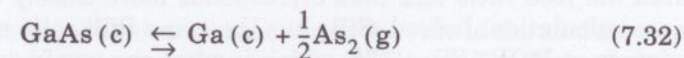

$$GaAs(c) \leftrightarrows Ga(c) + \tfrac{1}{2}As_2(g) \qquad (7.32)$$

for which $K = \sqrt{p(As_2)/p_o}$. This means that if $p(As_2)$ falls below the value required for equilibrium ("undersaturated"), GaAs will decompose to Ga in an attempt to raise $p(As_2)$. Conversely, if $p(As_2)$ is held above that value ("supersaturated"), GaAs will remain the only condensed phase. This situation was illustrated in the p_v diagram of Fig. 4.7, where the lower As_2 line represents the phase boundary between GaAs only (above the line) and GaAs + Ga (below). This is a simple example of a "CVD phase diagram."

A more complex phase diagram is shown in Fig. 7.14, where equilibrium calculations [17] show four depositing phases appearing in different domains of substrate T and gas-feed ratio. The silicon-boride phases that are richer in B occur for higher BCl_3/SiH_4 feed ratio, as one would expect. The gas ratio within which one obtains pure SiB_3 is especially narrow. Experimentally, the SiB_3 phase was actually ob-

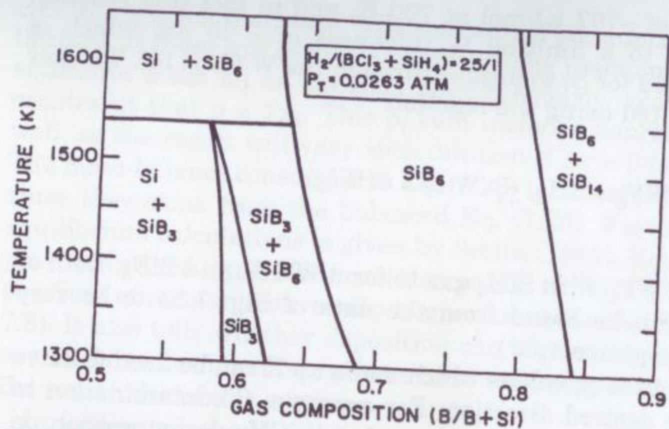

Figure 7.14 Calculated equilibrium CVD phase diagram for deposition of Si borides from $BCl_3 + SiH_4$. (Source: Reprinted from Ref. 17 by permission.)

tained at a much higher B/(B + Si) feed ratio of 0.75, rather than at 0.6 as shown. The likely explanation for this discrepancy [17] arises from the observation in Fig. 7.14 that the boride deposits are all richer in B than the feed gas mixture according to the equilibrium calculation. This means that if the deposition rate is being limited by the diffusive transport of gas to the surface, the gas composition at the surface will become more depleted in BCl_3 than in SiH_4 as the BCl_3 is preferentially consumed in deposition. That is, the *effective* gas ratio is lower than the feed ratio and thus corresponds more closely to the equilibrium calculation. Indeed, SiB_3 has the same B/Si ratio as the feed gas mixture at B/(B + Si) = 0.75, which is what one would expect for diffusion-limited deposition with similar diffusivities for the two gases. Here, the experimental CVD phase diagram is said to be "transport-shifted" relative to the equilibrium one. This example points up the major shortcoming of equilibrium calculations in CVD work, which is that equilibrium is seldom achieved. Diffusion-limited deposition will be discussed further in Sec. 7.4. A second impediment to the achievement of equilibrium is reaction rate, which we will discuss next.

7.3.2 Gas-phase rate

The source gases usually begin to decompose and/or react with each other as soon as they become hot enough during transport through the reactor, and before they adsorb on the surface of the depositing film. The extent of this homogeneous reaction depends both on the flow pattern and on the reaction rate, and it must be controlled in order to achieve good CVD.

In Secs. 5.1 and 5.2, we developed some principles of reaction kinetics for first-order adsorption and surface-diffusion reactions. The same principles apply here in the gas phase. The rate of a first-order gas-phase reaction per unit volume may be written as

$$R_+(\mathrm{mc/m^3 \cdot s}) = k_+ n_A = k_+ \frac{p_A}{k_B T} \tag{7.33}$$

and that of a second-order gas-phase reaction as

$$R_+(\mathrm{mc/m^3 \cdot s}) = k_+ n_A n_B = k_+ \frac{p_A p_B}{(k_B T)^2} \tag{7.34}$$

Here, subscript (+) denotes the forward direction in a reversible reaction such as Eq. (7.25), and $n_{A,B}$ are the reactant concentrations in mc/m^3. The conversion to partial pressures $p_{A,B}$ assumes the ideal-gas law [Eq. (2.10)]. Note that the units of the rate constant, k_+, will depend on the reaction order, and that k_B must be in J/mc · K.

It is important to recognize that the order of a reaction is not just the sum of the reactant coefficients, ν_i, in the stoichiometric equation [such as Eq. (7.25)]. This is because such an equation represents an *overall* reaction, which generally involves more than one reaction step. For example, Fig. 7.15 maps the reactions believed to be important in the deposition of Si from silane by the overall reaction

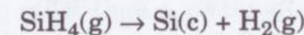

$$SiH_4(g) \rightarrow Si(c) + H_2(g)$$

In general, the rate of an overall reaction is the rate of the *slowest* step in the *fastest* of various parallel reaction pathways. The fastest path-

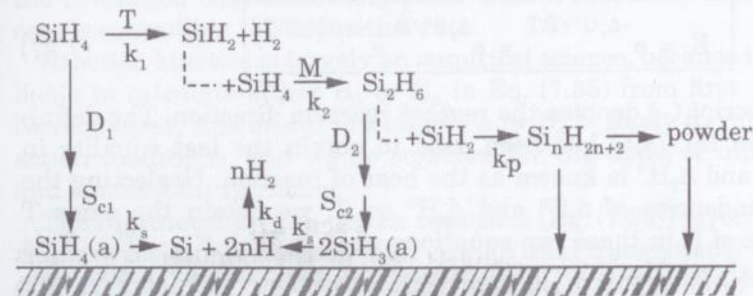

Figure 7.15 Gas-phase and surface reactions believed to be important in the thermal deposition of Si from SiH_4 gas: k_i = reaction rate constants, M = third body in a reactive collision, D_i = gas diffusivities, and S_{ci} = sticking coefficients.

way dominates, and the slowest step in that pathway limits its rate. The reaction order is then determined by the number of intermediate species that are reactants for that particular step. Thus, for example, reaction Eq. (7.31) for W deposition is not third-order in H_2 and first-order in WF_6 for a total of fourth-order, as implied by the v_i values, but in fact has been determined experimentally [16] to be half-order in H_2 and zeroth order in WF_6. This suggests that the rate-limiting step in this case is dissociative adsorption of H_2 on W: $(1/2)H_2(g) \rightarrow H(a)$. Fourth-order reaction implies the simultaneous collision of four reactant molecules (here, one WF_6 and three H_2 molecules) with enough energy and collision time to allow for their complete bond rearrangement into products. Clearly, this is an unlikely event, and in fact most reactions are second-order or less.

The general form of the Arrhenius expression for the rate constant, which was derived as Eq. (5.16) for surface diffusion, applies to all reactions; that is,

$$k_+ = B_+ e^{-E_a/RT} \tag{7.35}$$

where E_a is the activation energy per mole, and where the factors constituting the pre-exponential factor B_+ depend on the type of reaction, as we will see below. Equation (5.31) for K also holds here, so that we may write

$$K = \frac{k_+}{k_-} = \frac{B_+}{B_-} e^{-(E_{a+} - E_{a-})/RT} \tag{7.36}$$

and

$$\boxed{K = e^{-\Delta_r G^\circ/RT} = e^{\Delta_r S^\circ/R}\, e^{-\Delta_r H^\circ/RT}} \tag{7.37}$$

where subscript (–) denotes the reverse reaction direction. The definition of G in Eq. (4.5) has been used to obtain the last equality in Eq. (7.37), and $\Delta_r H^\circ$ is known as the heat of reaction. Neglecting the small dependencies of $\Delta_r S^\circ$ and $\Delta_r H^\circ$ on T, we obtain the same T dependence of K in these two equations when $\Delta_r H^\circ = E_{a+} - E_{a-}$. This fundamental relationship is illustrated in the familiar activation-energy diagram of Fig. 7.16. Note that a thermodynamically favorable reaction (negative $\Delta_r G^\circ$) may have a $\Delta_r H^\circ$ of *either* sign, depending on the entropy change, $\Delta_r S^\circ$. Reactions having positive $\Delta_r H^\circ$ absorb heat (they are "endothermic"), and their K increases with T. "Exothermic" reactions behave just the opposite. $\Delta_r H^\circ$ may be calculated from H°

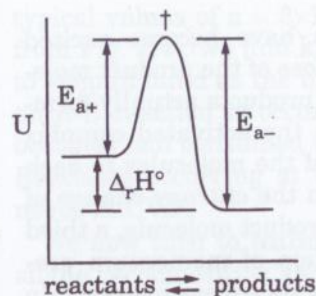

Figure 7.16 Activation-energy diagram for an exothermic reaction. The (†) at the top of the hill represents the energy level of the activated complex, and U is the internal energy of Σv_i moles in Eq. (7.25).

values found in handbooks [11, 12] or in various on-line data bases [13]. By the way, since only *relative* heat content can be measured, the H° of all species is specified to be zero at 298 K. Relating E_{a+} and E_{a-} to thermodynamics in the above way only tells us their difference, $\Delta_r H^\circ$, unfortunately. Thus, we encounter the first difficulty of reaction kinetics: finding E_a.

The slope of an experimental Arrhenius plot, $\log_{10} R_+$ versus 1/T (K), is frequently used to calculate an E_a using Eqs. (7.33) through (7.35) or the equivalent equations for surface reactions. In thin-film work, the R_+ measured is generally the deposition rate (mc/cm^2·s). The significance of such an *apparent* E_a must be viewed with some caution. Often, it is not known which reaction step is the rate-limiting one, nor even what are the elementary reaction steps. If two steps have similar rates, the E_a will be an average of the two and is likely to change with T. Often, something *other* than a reaction rate is controlling the film deposition rate, such as diffusion of reactants to the surface (Sec. 7.4) or the supply of activated species from a plasma (Sec. 9.6). In both of these cases, a very low and physically meaningless E_a will be obtained from the Arrhenius plot, and then the value of the plot becomes simply the revelation that something other than a thermally activated process is controlling the deposition rate.

Reaction kinetics is largely an empirical science, because it is not reliable to calculate either B_+ or E_a in Eq. (7.35) from first principles. Nevertheless, it is useful to examine how B_+ is likely to vary with reaction conditions, and we do so below for the cases of unimolecular and bimolecular reactions.

The **bimolecular gas-phase reaction** [Eq. (7.34)] involves the two reactant molecules colliding with enough total translational kinetic energy, ε_t, along the direction of their mutual approach to surmount the E_a "hill" of Fig. 7.16. We saw in Sec. 2.2 that the probability of a molecule having energy ε_t in a given direction is proportional to $\exp(-\varepsilon_t/k_B T)$, and this is the origin of the exponential factor in the Arrhenius equation. The top of the E_a hill represents the "activated complex" in

which the bonds of the reactant molecules have become excited enough vibrationally by the collision so that those of the product molecules can begin to form. The probability of the products actually forming instead of the reactants re-forming when the activated complex decomposes depends both on the orientation of the molecules to each other upon collision (the "steric" factor) and on the entropy change of the reaction. In cases where there is only one product molecule, a third probability factor appears, because conservation of momentum prevents the activated complex from transferring its excess energy into translational kinetic energy of the products. To prevent this energetic product molecule from decomposing, its energy must instead be transferred in a collision with a nonreacting "third body" before the decomposition has time to occur. The third body can be either a nonreacting gas-phase molecule/atom or a surface. When it is a molecule or atom, the rate constant increases with total pressure as well as with the reactant concentrations n_A and n_B, so that the reaction exhibits "pseudo-third-order" kinetics. None of the above three probabilities can be predicted accurately, so they are accounted for together by a "fudge" factor, s, in the rate expression:

$$R_{II}\left(mc/cm^3 \cdot s\right) = s\, e^{-E_a/RT} R_c = s\, e^{-E_a/RT} k_c n_A n_B = k_{II} n_A n_B \qquad (7.38)$$

where subscript II denotes a bimolecular reaction; R_c is the collision rate per unit volume between the two reactants, A and B; and k_c is the collision rate constant.

The upper limit of the gas-phase bimolecular reaction rate occurs when s is unity and $E_a << RT$. In that case, $k_{II} \rightarrow k_c$, and the reaction is said to be proceeding at "collision rate." This rate, at least, can be calculated easily from the gas kinetic theory of Chap. 2. The collision frequency (collisions/s) of some individual molecule with any other molecule is $\bar{c}/l$, where the mean speed, $\bar{c}$, and the mean free path, l, were given by Eqs. (2.3) and (2.24). This frequency times n_A is the collision rate of species A with any other molecule, per unit volume, and this rate times the fraction of B in the gas mixture, n_B/n, is the A-B collision rate, R_c ($mc/cm^{-3} \cdot s^{-1}$). Combining all of this, we have

$$R_c = \sqrt{\frac{8RT}{\pi M_r}} \left(\sqrt{2}\pi \overline{a^2} n\right) n_A \frac{n_B}{n} = \left[\sqrt{\frac{\pi RT}{M_r}}\, 4\overline{a^2}\right] n_A n_B \qquad (7.39)$$

where $\overline{a^2}$ is the mean-square collision diameter of the A-B pair, and $M_r = 2M_A M_B/(M_A + M_B)$ is its "reduced" mass. Comparison with Eq. (7.38) shows that the term in brackets is the k_c that we seek. For typical values of $a = 3\times10^{-8}$ cm and $\bar{c} = 4\times10^4$ cm/s (for Ar at 298 K from Fig. 2.4), we find $k_c = 1.6\times10^{-10}$ $cm^3/mc \cdot s$, a very useful number to keep in mind as the upper limit of bimolecular reaction rate. When an A-B reaction is occurring at collision rate, the deficient reactant becomes half consumed within the travel time between A-B collisions. Reactions occurring at this rate may be considered to be instantaneous in CVD.

We now turn to **unimolecular gas-phase reactions** such as the silane decomposition shown as k_1 in Fig. 7.15. Although the term unimolecular implies spontaneous decomposition, the rate is governed by collisions with nonreactive neighbors, because that is how a gas molecule gains enough internal energy to dissociate—at least in a thermally controlled reaction. Having gained enough energy to reach the top of the E_a hill of Fig. 7.16, the molecule then dwells for some time, t_e, in that activated state until the internal energy, in its statistical ramblings, happens to concentrate itself into the vibrational mode(s) leading to dissociation. If t_e is less than the mean time between collisions, which is $t_c = l/\bar{c}$ (mean free path/mean speed), then the molecule is likely to dissociate before the next collision. Thus, when $t_e < t_c$, the unimolecular dissociation rate per unit volume, R_I, increases not only with concentration n_A, but also with collision frequency and, therefore, with total pressure. That is,

$$R_I \propto p n_A \qquad (7.40)$$

By comparison with Eq. (7.34), we can see that this reaction is behaving as a first-order reaction with $k_I \propto p$, or as a "pseudo-second-order" reaction. More complex molecules have longer t_e due to their larger number of internal-energy modes. Also, $t_c \propto 1/p$, so at high enough p, t_c becomes less than t_e. Then, the activated molecule is just as likely to lose energy as to gain it in the second collision, so further increase in p does *not* increase the rate at which reactant molecules achieve dissociation energy. This is the "high-pressure limit," where k_I becomes independent of p, and the unimolecular dissociation reaction exhibits true first-order kinetics.

It should now be clear why it is not possible to predict gas-phase k_i values from first principles. Similar complications arise for surface reactions, as we discovered in Sec. 5.2 by examining the simplest possible surface "reaction"—the hopping of an adsorbed molecule from one bonding site to another. Therefore, the kinetically favored pathways in a CVD reaction map such as that of Fig. 7.15 must be determined experimentally. The kinetic modeling approach to this problem is often used in CVD process studies. This involves proposing a likely reaction pathway and then fitting its k_i values to data for deposition rate ver-

sus p_i, p, and T. However, Fig. 7.15 shows that even for a simple overall CVD reaction having only one reactant and one gaseous product, there are many k_i terms, including also the sticking coefficients, S_{ci}, of the depositing precursors. Even the diffusivities, D_i, of the precursors may limit deposition rate at high p. Fitting CVD data by adjusting many k_i values is like fitting a wavy line to a polynomial: it is always possible, but there is no chemistry involved. That is to say, the achievement of a fit does not mean that one has correctly identified the reaction pathway or correctly calculated the k_i values of the individual reaction steps.

The second and more fruitful approach to the k_i values is to actually measure them individually. This difficult and tedious task has not been carried out for most CVD reactions, but it must be done to fully understand a chemical process. One way is to generate a burst of a single reactive-intermediate species by flash photolysis (light-induced dissociation) and then track its disappearance transient using some species-selective probe such as laser-induced fluorescence. For example, it has been found using this approach [18, 19] that the insertion reactions of silylene (SiH_2) into SiH_4 and Si_2H_6 shown in Fig. 7.15 by k_2 and k_p proceed at collision rates. The first reaction requires a third body (denoted by M), but k_2 was found to reach k_c by the time p reached only 130 Pa using He diluent. Significantly, these k_i values are *orders of magnitude* higher than previous estimates made by kinetic modeling. This result establishes that the gas-phase reaction rate in silane pyrolysis is governed by k_1, the unimolecular dissociation of silane. Under Si CVD conditions where k_1 was believed to be controlling deposition rate [20], rate analysis yielded $k_1 = 0.35\ s^{-1}$.

A certain amount of gas-phase reaction is sometimes required to partially decompose the feed gases and thereby render them sufficiently reactive when they arrive at the film surface, as in the case of the $(CH_3)_3Ga$ and AsH_3 used in GaAs deposition. However, if the sticking coefficients, S_c, of these gas-phase products are too high, they will adsorb before they can diffuse between the stacked substrates of the batch reactor (Fig. 7.6c) or down into the crevices of rough substrates. This results in poor uniformity of film coverage, as we will see in the next section. Excessive gas-phase reaction also usually leads to gas-phase nucleation of film material as powder which can contaminate the film surface and which depletes the reactant supply ("parasitic" reaction). In Si deposition from silane, powder formation occurs by the successive insertion of SiH_2 into Si_nH_{2n+2} as shown by the polymerization rate constant k_p in Fig. 7.15. The rate of each step is second-order in concentration [Eq. (7.34)] and also increases with the dissociation rate of SiH_4 into SiH_2, which increases with both $p(SiH_4)$ and total p [Eq. (7.40)]. The resulting strong p dependence of powder

formation leads to the observation of a critical $p(SiH_4)$, above which it becomes noticeable. In one study [21] at $T_s = 1000$ K and with a 1-s residence time of undiluted SiH_4 in the reactor, the critical $p(SiH_4)$ was found to be about 130 Pa.

The extent of any gas-phase reaction occurring within a CVD reactor is proportional to residence time and rate. Residence time, t_r, in the *entire* reactor volume, V_r, is given by

$$t_r = \frac{V_r}{W} = \frac{V_r}{(Q/p)(\bar{T}/273)} \tag{7.41}$$

where W (cm³/s) = total volume flow rate of gas
Q (sccs) = total mass flow rate of gas
p (atm) = reactor pressure
$\bar{T}$ (K) = volume-average T in reactor

Except in isothermal reactors, only some smaller volume, V_h, is heated enough that reaction proceeds at a significant rate. Then, the fraction of t_r which the reactant spends in that volume is V_h/V_r when diffusional mixing is fast (low p). When mixing is slow (high p), V_h/V_r instead roughly represents the fraction of reactant that passes through V_h rather than passing around it. In either case, the fractional exposure of reactant to the "hot zone" is roughly the same. When, in addition, the fractional consumption of reactant, ξ, is small enough so that one does not need to use integration to follow the kinetics, and when the reacted composition is far enough from equilibrium so that the reverse reaction is negligible, then the amount of reactant A consumed in the controlling gas-phase reaction of rate R_g is simply

$$\Delta n_A = R_g t_r (V_h/V_r) \tag{7.42}$$

Assuming further, for simplicity, that the kinetics are first-order in A, we then obtain from Eqs. (7.33), (7.41), and (7.42) a very useful qualitative expression for fractional reactant consumption in the gas phase:

$$\xi = \frac{\Delta n_A}{n_A} = \frac{k_I V_h}{Q} \frac{p}{p^\circ} \frac{273}{\bar{T}} \tag{7.43}$$

Note that another p factor due to residence time has been added to the one already incorporated into k_I.

The above two equations suggest other ways to reduce ξ besides decreasing p. One way is to decrease t_r by increasing Q. However, if t_r is made too small, reactant will not have time to diffuse to the surface or to encounter enough collisions there to react before being swept down-

stream. The other way is to decrease the hot-zone volume, V_h. The size of V_h varies considerably with reactor design and flow pattern. Clearly, the worst case is the isothermal batch reactor of Fig. 7.5c. Nevertheless, particles can be avoided in this reactor if p is sufficiently low, and the good substrate-T control of the isothermal reactor makes it useful for deposition-rate uniformity.

In cold-wall reactors, the roll cells which can occur in the flow pattern (Figs. 7.7 and 7.12) cause V_h to increase toward V_r by convectively carrying heat away from the substrate region. When these cells are avoided, V_h is instead restricted to the region of steep T gradient adjacent to the substrate surface, which is shown by Θ for the rotating-disc situation in Fig. 7.11. This steep T gradient not only minimizes V_h, but also greatly simplifies process modeling by allowing the use of the "chemical-boundary-layer" concept [22]. There, the reaction zone is approximated as a layer of uniform $T = T_s$ and of thickness δ_c against the substrate surface. The value of δ_c is adjusted so that the same amount of reaction occurs as that which would occur integrated over the actual T gradient. This concept conveniently separates the gas-phase-reaction step of the process from the convective-transport step, whereas the treatment of these two steps together amidst T gradients is a formidable problem. For the case of parabolic flow in a horizontal-tube reactor of height y_o, δ_c can be approximated by the following equation [22] when the activation energy, E_a, for the rate-limiting gas-phase reaction is >100 kJ/mol:

$$\frac{\delta_c}{y_o} = \frac{(1+\beta)\,(T_s/T_\infty)^{1+\beta}}{(T_s/T_\infty)^{1+\beta}-1}\,\frac{RT_s}{E_a} \approx \frac{16}{E_a\,(\mathrm{kJ/mol})} \qquad (7.44)$$

Here, β comes from $K_T \propto T^\beta$, where K_T is the gas thermal conductivity. When heat capacity $c_v \neq f(T)$, $\beta = 0.5$ by Table 2.1. For a more typical value of $\beta = 0.7$, for $T_s = 1000$ K, and for $T_\infty = 300$ K, we obtain the last equality in Eq. (7.44). This is a useful way of making a rough estimate of hot-zone volume and therefore of the extent of gas-phase reaction.

7.3.3 Surface processes

The surface processes of CVD are adsorption of the source gases, surface diffusion, heterogeneous reaction of the adsorbates with each other and with the surface, and desorption of gaseous by-products, as shown for Si deposition in Fig. 7.15. Four quantities are used to describe the fractional consumption of reactant impinging with flux J_i on the surface, as discussed in Sec. 5.1 and Fig. 5.1. These quantities must be carefully distinguished in describing CVD, but there is some

discrepancy in the literature. Here, we define them as follows, in order of increasing amount of interaction with the surface. The **trapping probability,** δ, is the fraction of J_i that physisorbs into the precursor state instead of being immediately reflected from a clean surface, a clean surface being one whose bonding sites are all free of adsorbate. The vapor may subsequently desorb from the precursor state without reacting. The **chemisorption-reaction probability,** ζ, is the fraction of J_i that does react into a chemisorbed state with the clean surface. It may subsequently react back into a precursor state and desorb, or it may remain and become part of the film. The **sticking coefficient,** S_c, is the fraction of J_i that remains adsorbed long enough to become buried and thus permanently incorporated into the depositing film. Its value is averaged over the *whole* surface, both clean and adsorbate-occupied portions. The S_c will be less than ζ when some of the chemisorbed reactant is desorbing or when part of the surface is passivated against adsorption by being already occupied with adsorbate. Finally, the **utilization fraction,** η, is that fraction of the vapor entering the reactor that becomes incorporated into the film instead of being carried downstream and pumped away. Since there are many encounters of a vapor molecule with the surface, η can be high even when the other fractions are low.

Adsorption and reaction of a single species were considered in Sec. 5.1, where Eq. (5.7) for ζ was derived for conditions of vanishingly small and steady-state precursor surface concentration and irreversible chemisorption reaction. For that case, $\zeta \equiv S_c$. Studies on clean, hot Si under ultra-high vacuum [18, 23] approximate these conditions and have shown that the S_c of Si_2H_6 is much higher than that of SiH_4. This points up the importance of knowing the extent of gas-phase reaction (here $SiH_4 \rightarrow Si_2H_6$) in analyzing CVD kinetics. Thus, the deposition rate of Si from SiH_4 is found [24] to increase with total pressure, p, and residence time, t_r [Eq. (7.41)], at fixed $p(SiH_4)$ due to an increasing amount of gas-phase reaction with increasing p and t_r as discussed prior to Eq. (7.41).

In general, the surface concentrations of precursors and reaction by-products in CVD *cannot* be neglected as they were for Eq. (5.7). They can inhibit further adsorption or drive surface-reaction equilibrium one way or the other. Regarding by-product buildup, for example, H bonds very strongly to the Si surface and passivates it against any adsorption, as pointed out in Sec. 6.3, so that S_c is much lower on an H-covered Si surface than on a clean one. In fact, the H desorption reaction, $2H(a) \rightarrow H_2(g)$, is believed to be the rate-limiting surface step in Si CVD [18] at low pressure where the gas-phase decomposition of SiH_4 is small. A plot of deposition rate versus 1/T under these

conditions then measures the E_a of H_2 desorption and gives $E_a \approx 200$ kJ/mol.

As in the gas phase, surface-reaction rates are determined by the surface concentrations of the reactants, n_s (mc/cm^2), in accordance with the rate equations, Eqs. (7.33) and (7.34) (written there for the gas phase). We now consider the steady-state n_s of a single reactant A as a function of its partial pressure, p_A, at some fixed surface T, assuming for the moment a negligible loss rate by film-forming reaction. Such a function is known as an "adsorption isotherm" and is analogous to the n-p behavior at fixed T for a gas, either ideal [Eq. (2.10)] or nonideal (Fig. 2.1). To derive a typical isotherm, we start with the Langmuir adsorption model of Sec. 6.5.5, in which adsorption is assumed to occur only on unoccupied surface sites. In Sec. 6.5.5, we also assumed a fast chemisorption reaction (that is, $\zeta \rightarrow \delta$) that was irreversible (no desorption), and this resulted in an asymptotic approach of n_s to monolayer coverage: $\Theta = n_s/n_{so} = 1$. Those assumptions were appropriate for the adsorption of a reactant upon a surface with which it bonds strongly. Here, we instead want to examine precursor reactions on less reactive surfaces, so we neglect the chemisorption reaction and add to the Langmuir model a finite desorption rate obeying first-order kinetics with a rate constant k_d. The steady-state mass balance on the surface thus becomes

$$J_i\delta(1-\Theta) = k_d n_s = k_d n_{so}\Theta \tag{7.45}$$

which is also the limiting form of the Eq. (5.3) mass balance as the chemisorption rate constant, k_r, vanishes. From the Knudsen equation [Eq. [2.18)], we know that $J_i \propto p_A$, so adsorption on the clean surface may be thought of as a first-order reaction with $J_i\delta = k_a p_A$. Here, the $1/k_BT$ factor from Eq. (7.33) has been incorporated into k_a. Solving Eq. (7.45) for Θ and using this expression for $J_i\delta$ gives the equation for the Langmuir isotherm:

$$\boxed{\Theta = \frac{n_s}{n_{so}} = \frac{p_A}{\left(\dfrac{k_d n_{so}}{k_a}\right) + p_A}} \tag{7.46}$$

Inspection of this equation and its plot in Fig. 7.17 shows a linear region where $\Theta \propto p_A$ at low p_A, and a saturation region where Θ is independent of p_A at high p_A. These limiting regions are observed for all isotherms, not just for the Langmuir model, provided that $p_A < p_v$ so that bulk condensation does not occur. For CVD, the limiting behaviors are more important than the exact shape of the curve in between.

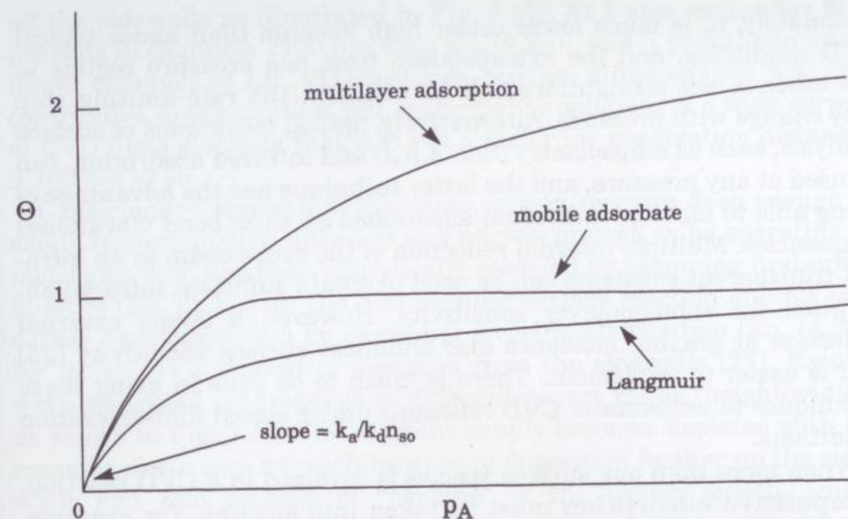

Figure 7.17 Typical adsorption isotherms: $\Theta = n_s/n_{so}$ = fractional monolayer surface coverage.

Two common variations from Langmuir behavior are also shown in Fig. 7.17. Observation of the mobile-adsorbate effect shown was cited after Eq. (6.20). The other variation involves adsorption beyond 1 ML, as embodied in the BET (Brunauer-Emmett-Teller) and other isotherms developed in the study of heterogeneous catalysis.

Now that we have established a formalism for describing adsorption and surface coverage in CVD, we will examine five effects of adsorbate concentration, n_s, on film deposition behavior, namely: pressure dependence of deposition rate, competitive adsorption, film conformality over topography, roughening, and selective deposition.

The behavior of n_s versus p_A, as embodied in the adsorption isotherm, is reflected in **film deposition rate versus p_A** in cases where the surface reaction is controlling the rate rather than another step in the Fig. 7.1 sequence. That is, the rate typically increases with p_A and then saturates at high p_A. For high δ and low k_d in Eq. (7.45) corresponding to strong adsorption, coupled with a low rate of the film-forming reaction [k_r in Eq. (5.5)], this saturation can occur at very low p_A even into the Kn > 1 regime (see Exercise 7.10). The nonlinear behavior of n_s versus p_A also points up a problem with extrapolating high-vacuum studies of surface-reaction kinetics to CVD behavior at higher pressure. High vacuum with Kn >> 1 is required for such studies, since they typically involve modulated-molecular-beam techniques (Fig. 6.9) or surface analysis by electron spectroscopy (Sec. 6.4.1). Un-

fortunately, n_s is much lower under high vacuum than under typical CVD conditions, and the extrapolation from one pressure regime to the other is not straightforward. In addition, the rate-limiting step may *change* with pressure. Alternatively, optical techniques of surface analysis, such as ellipsometry (Sec. 4.8.2) and infrared absorption, can be used at any pressure, and the latter technique has the advantage of being able to monitor individual adsorbates by their bond vibrational frequencies. Multiple internal reflection of the probe beam in an infrared-transparent substrate can be used to obtain sufficient infrared absorption for submonolayer sensitivity. However, a single external reflection at grazing incidence also enhances surface sensitivity [25] and is easier to implement. There is much to be done in using these techniques to understand CVD reactions under actual film-deposition conditions.

When more than one surface species is involved in a CVD reaction, **competitive adsorption** must be taken into account. For example, the deposition rate of Si is greatly reduced when a small amount of PH_3 or AsH_3 is added to the reactant feed to n-dope the Si, because the adsorption of these reactants passivates the surface against SiH_4 adsorption (see references cited in Ref. 20). The curious and troublesome phenomenon of multiple steady states of reaction behavior [26] has also been explained by competitive adsorption in the case of $TiCl_4$ and C_3H_8 reacting in the adsorbed state (Langmuir-Hinshelwood mechanism) to form TiC film and HCl gas. As the partial pressure of $TiCl_4$, $p(TiCl_4)$, is raised, deposition rate and p(HCl) at first increase due to increasing $n_s(TiCl_4)$. At some level of $p(TiCl_4)$, however, deposition rate and p(HCl) suddenly drop to a much lower level, because excessive $n_s(TiCl_4)$ is preventing adsorption of the other reactant, C_3H_8. When $p(TiCl_4)$ is then decreased, hysteresis is observed: that is, rate and p(HCl) remain low and then finally jump up at some lower $p(TiCl_4)$. Clearly, these situations must be understood to achieve good process control.

Good **film conformality** over surface topography is one of the principal features of CVD, but it does not always occur. Conformality becomes harder to achieve when the recessed regions into which one wants the deposit to penetrate have a lateral dimension less than that needed for convective transport into them. Then, penetration can occur only by diffusive transport through the stagnant gas, as will be discussed in Sec. 7.4. This is the situation, for example, for the spaces between the stacked wafers of the batch reactor of Fig. 7.5*c*. When the lateral dimension of the recess is still smaller—less than the gas mean free path, diffusion no longer slows down the penetration, but still the reactant becomes progressively depleted by deposition onto the sidewalls of the recess as it penetrates deeper by molecular flow, bouncing

off the sidewalls as illustrated in Fig. 5.17*f*. At 1 atm, molecular flow prevails in channels <100 nm wide Eq. (2.24)], and it prevails in much larger channels at LPCVD pressures. Surface diffusion (Sec. 5.2) also contributes to penetration, but conformality behavior of a wide variety of CVD films suggests that it is not a factor for penetration distances > 100 nm or so.

Conformality versus film thickness, within recesses deep enough to safely neglect surface diffusion and narrow enough to be operating in molecular flow, has been analytically modeled by assuming first-order kinetics [Eq. (7.33)] for the film-forming surface reaction and for precursor desorption, and by assuming a cosine distribution [Eq. (4.30)] for molecules scattered or desorbed from the sidewalls [27]. Results were computed for trenches of different aspect ratios (height/width), as shown in Fig. 7.18. The reactant supply becomes depleted with increasing depth into a trench because of deposition further up the sidewalls and also because of "necking" of the trench mouth, which narrows the solid angle from which deeper regions can receive deposition flux. Clearly, for good conformality one wants a low sticking coefficient, S_c, for the reactant so that most of it can bounce down to the bottom of the trench. When deposition conditions are such that the fractional surface coverage, Θ, of precursor is low, then $S_c \equiv \zeta$, where ζ is the reaction probability of a molecule impinging on bare surface as defined in Eq. (5.7). Figure 7.18*a* shows trench coverage computed for $\Theta = 0$ and $\zeta = 0.10$ (although the notation and terminology are different in the referenced work). The poor coverage for the deeper trenches shows that ζ needs to be still lower to obtain good coverage under conditions of low Θ, which is the "adsorption-limited" regime of deposition rate. Lower ζ can be achieved by reducing surface T. When Θ is higher, on the other hand, S_c becomes low even if ζ is high, since precursor is

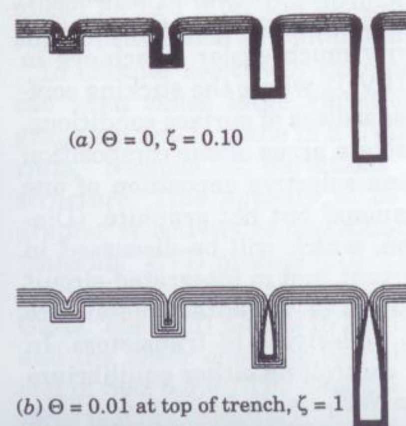

Figure 7.18 Calculated film-conformality profiles in trenches. (Source: Reprinted from Ref. 27 by permission.)

assumed not to adsorb on surface already covered. Figure 7.18*b* shows trench coverage for $\Theta = 0.91$ at the mouth of the trench and for $\zeta = 1$. [Θ becomes lower inside the trench due to depletion of reactant incident flux and partial pressure, p_A, in accordance with Eq. (7.46).] The figure shows that Θ needs to be still higher to obtain good coverage. This can be achieved by operating at higher p_A, further into the adsorption-saturation regime of the Eq. (7.46) isotherm. This is the "surface-reaction-limited" regime of deposition rate. However, if high p_A causes gas-phase reactions to form powder or high-S_c precursors, this remedy becomes less workable. The trench conformality problem is often encountered in integrated-circuit manufacture. It also occurs when coating the internal surface area of porous materials (see Exercise 7.15). Deposition into trenches or into cavity structures such as that of Fig. 9.35 is a good way to determine the S_c of film precursors.

Reactant depletion in recessed areas due to high S_c also aggravates **film roughening**, a topic discussed at length in Sec. 5.4.1. To summarize that discussion, substrate roughness and statistical roughening initiate the process, which is then amplified by "self-shadowing" for high S_c or by "nutrient (reactant) depletion" for low S_c. These are actually two names for the same phenomenon in different S_c ranges, that phenomenon being removal of reactant from the vapor phase by deposition. In either case, it is inherently destabilizing to surface smoothness, because the deeper the roughness features become, the more depletion there is, the slower the deposition rate is at the bottom relative to the top, and thus the faster the roughness develops. Surface diffusion is the counteracting phenomenon which stabilizes the smooth surface, and the final amplitude and scale of the roughness represent the balance between depletion and diffusion [28].

The achievement of **selective deposition** is largely determined by control of adsorbate surface coverage, n_s. The wide range of adjustability in n_s and the presence of large activation energies for the reaction of source gases together make selectivity much easier to achieve in CVD than in physical vapor deposition (PVD), where the sticking coefficients of most vapors are near unity, regardless of surface conditions. Selectivity can mean deposition on substrate areas of one composition while not on other areas, or it can mean selective deposition of one solid phase and not others, such as diamond but not graphite. (Diamond deposition uses plasma activation, which will be discussed in Chap. 9.) Area selectivity is a very important goal in integrated-circuit manufacture, as in the selective deposition of W contact metal into vias etched through SiO_2 film down to underlying Si transistors. In general, selectivity may be obtained by controlling either equilibrium or kinetics. Selective W deposition from WF_6 on Si, but not on SiO_2, was mentioned after Eq. (7.30) and is an example of equilibrium control, since there is no favorable W-deposition reaction on SiO_2. But since the reaction on Si consumes the Si, it is self-limiting, and thick deposits thus require the addition of H_2 or SiH_4 to chemically reduce the WF_6. There, deposition on SiO_2 can still be avoided, but now it is due to a *kinetic* limitation. Let us assume that the film-forming reaction is second-order in reactant surface coverage, n_s, with a rate given by $R_r = k_r n_s(WF_6) n_s(H_2)$. In the absence of chemisorption reaction with the SiO_2, these molecules will only physisorb and will thus both have low n_s because of a high k_d and possibly also a low k_a in Eq. (7.46) for surface coverage. Nevertheless, R_r is not zero, so W nuclei will eventually form after some "incubation time." Subsequent deposition on these nuclei is much faster, probably due to a lowering of the reaction's E_a by dissociative adsorption [16] of H_2 on W. Thus, selectivity is quickly lost once nuclei form. The surface W is acting here as a catalyst to activate the H_2. Nucleation behavior was discussed at length in Sec. 5.3.

Deposition on undesired areas or deposition of unwanted phases can also be avoided by raising the surface coverage of a deposition-reaction *by-product* and thus driving the reaction in the reverse direction in accordance with equilibrium behavior [Eq. (7.28)]. For example, addition of HCl product improves selectivity in the deposition of Si from SiH_2Cl_2. Presumably, the $\Delta_r G°$ is less negative on SiO_2 than on Si because of weaker bonding of Si to SiO_2 than to itself; in other words, $\Delta_f G°[Si(a)] > \Delta_f G°[Si(c)]$ because of excess surface energy, γ_i, at the $Si(a)/SiO_2$ interface. Thus, with proper partial-pressure adjustment, a balance can be achieved where deposition is occurring on the Si while etching of Si nuclei by HCl is occurring on the SiO_2. H_2 plasma can also be used [29] instead of HCl to supply active etchant. The achievement of such an equilibrium balance is more reliable than kinetic control of selective deposition, because kinetic control breaks down at nuclei formed after the incubation time or formed at spurious active surface sites such as contamination islands or scratches.

In another selectivity example, a shift in $\Delta_r G°$ with surface energy can even cause large variations in deposition rate from crystallographic plane to plane in a CVD process that is operating near equilibrium, because of variations in surface energy, γ, with surface structure. This appears to be the cause of the dramatic crystallographic selectivity of deposition rate shown in Fig. 7.19 for the GaAs "chloride" CVD process [30]. There, GaCl, $AsCl_3$, and H_2 react to deposit GaAs, and at the same time the HCl(g) by-product etches the GaAs. The {111} planes in the upper hemisphere are the Ga-rich ones, and the lower ones are As-rich. (GaAs polarity was discussed at the end of Sec. 6.5.6.) The deposition-rate anisotropy between these polar faces is more than 15/1.

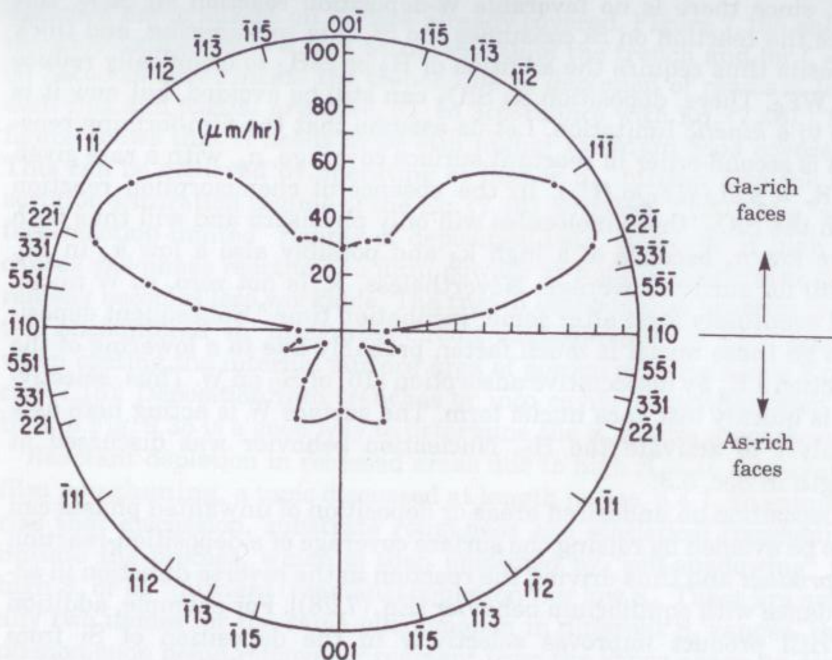

Figure 7.19 Polar diagram of GaAs deposition rate by the chloride process vs. crystallographic plane. (Source: Reprinted from Ref. 30 by permission.)

The final aspect of surface chemistry to discuss is the steep exponential T_s dependence of deposition rate which is induced when a surface reaction is the rate-controlling step of the CVD process. There are both advantages and disadvantages to this behavior. To obtain uniformity over large areas, the furnace-enclosed reactor of Fig. 7.5c is usually needed in order to obtain sufficient substrate-T control under such conditions. To compensate for the reactant depletion which occurs at substrates toward the downstream end of this reactor, an increasing T profile can be imposed along the furnace (Exercise 7.11).

In other reactors, the steep T dependence can be used to start and stop the deposition reaction abruptly by changing surface T. This feature has been exploited in a technique known as "limited-reaction" or "rapid thermal" processing, in which the substrate is rapidly heated by irradiation from a quartz-halogen lamp focussed through a quartz reactor wall. The substrate is then somewhat less rapidly cooled by thermal radiation when the desired film thickness has been reached [31]. This procedure minimizes the time at high T needed to deposit a given thickness, and it thus minimizes the amount of interdiffusion occurring between layers in a heterostructure.

A surface-T increase can also be obtained on selected areas of a substrate by directing there the focussed beam from a high-power laser, so that deposition occurs only in the irradiated areas. This is done in conjunction with conventional substrate heating to just below the deposition T, to minimize laser power and thermal shock. The laser can be programmed to scan and write arbitrary patterns of deposition for the generation of three-dimensional thin-film structures. When a short wavelength is used, there is also the possibility that photochemical activation is occurring [32] in addition to local heating; that is, direct breaking of a reactant bond due to absorption of photon energy in electron excitation. One way to identify a photo*chemical* versus a photothermal effect is to see if it still occurs at cryogenic T [33].

The above discussion of chemical reactions in CVD has presented the basic principles of equilibrium and kinetics for gas-phase and surface reactions. However, it has stopped short of attempting overall kinetic modeling, because good data on rate constants are usually unavailable. Even in the much-studied SiH_4 pyrolysis reaction, the important rates are known only for the gas phase. Nevertheless, understanding how reaction equilibria and rates vary with pressure and T is valuable in designing and optimizing CVD processes.

7.4 Diffusion

We now consider the final transport step in the CVD process sequence of Fig. 7.1: gas-phase diffusion of reactants to the substrate surface. Forced and free convection have carried the gases to the *vicinity* of the substrate, and sometimes there also has been some homogeneous reaction along the way. However, viscous friction requires that the convection velocity drop to zero at the surface whatever the flow profile, so the final transport of reactants to the surface has to occur by diffusion through a relatively stagnant boundary layer of gas.

The transition from convection to diffusion is gradual upon approaching the surface, but it is convenient to model this situation as two distinct regions: a convectively supplied reservoir of reactant, and a diffusive boundary layer between this reservoir and the surface. The surface on which film is depositing is a sink for the reactant, so the reactant concentration, n_A, just over the surface is always lower than that in the reservoir, n_∞. That concentration gradient drives the reactant diffusion flux, J_A, as shown in Fig. 7.20, and the edge of the *concentration* boundary layer in which this diffusion is occurring, δ_n, is arbitrarily but conventionally defined as the plane at which n_A has dropped by 1 percent from n_∞. We shall see that δ_n behaves very differently from δ_v, the *velocity* boundary layer, which was discussed in Sec. 7.2.2. Below, we will apply the boundary-layer model to the three reac-

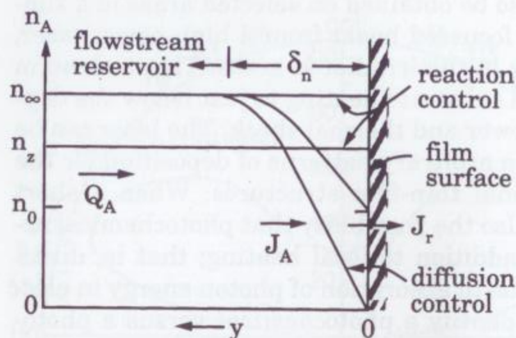

Figure 7.20 Quantities relevant to the diffusion of a single reactant, A, through the concentration boundary layer, δ_n, to the depositing-film surface at y = 0.

tors of Fig. 7.5. But first, we need to write the equations that describe diffusive transport.

In Sec. 2.8.1, we showed that the diffusion flux of species A in an A-B mixture is proportional to the concentration gradient by the binary diffusivity, D_{AB}, in accordance with Fick's Law, Eq. (2.27). When the total amount of gas remains constant, the countercurrent flux of B due to the displacement of B by A has to be equal and opposite to J_A, so $J_B + J_A = 0$. However, there is a complication in film deposition due to molarity changes upon reaction, such as $SiH_4(g) \rightarrow Si(c) + 2H_2(g)$. There, for every mole of SiH_4 diffusing to the surface and depositing Si, two moles of H_2 must diffuse away from the surface. This net flux of gas away from the surface, $J_B + J_A \neq 0$, is known as Stefan flow, and it sweeps A away from the surface in proportion to the mole fraction (or molecular fraction) of A in the mixture, $x_A = n_A/(n_A + n_B) = n_A/n$. Thus, the net flux of A toward the surface is the sum of the Stefan-flow and Fick's-law components:

$$J_A = x_A (J_A + J_B) - D_{AB}\frac{dn_A}{dy} \qquad (7.47)$$

or, rearranging and substituting x_B for $(1 - x_A)$ and nx_A for n_A,

$$\frac{dx_A}{dy} = \frac{x_A J_B - x_B J_A}{nD_{AB}} \qquad (7.48)$$

When generalized to three-dimensional diffusion of multicomponent mixtures, this becomes the Stefan-Maxwell equations [34]:

$$\nabla x_i = \sum_{j \neq i} \frac{1}{nD_{ij}} (x_i J_j - x_j J_i) \qquad (7.49)$$

When there are ν_p molecules of gaseous product per molecule of reactant deposited, Eq. (7.47) becomes

$$J_A = \frac{-D\frac{dn_A}{dy}}{1 + x_A(\nu_p - 1)} \qquad (7.50)$$

This reduces to Fick's Law for the equimolal counterdiffusion case ($\nu_p = 1$) or for high dilution ($x_A \rightarrow 0$). By contrast, consider conditions leading to large Stefan flow; that is, $\nu_p = 2$, no dilution, and all reactant being deposited ($x_A = 0$ at $y = 0$). Then, we may take the average x_A across the x_A gradient as 1/3, so that the denominator becomes 4/3. Thus, we see that this flow effect is noticeable but not enormous, and it may be neglected for rough calculations.

7.4.1 Diffusion-limited deposition

We wish to determine the degree to which the concentration gradient required for diffusion depletes the reactant over the surface and thereby limits the film-forming surface-reaction rate. We will assume that only one reactant is diffusion-limited, and we will thus will drop some of the A subscripts from above for simplicity. Using the boundary-layer model just introduced and referring to Fig. 7.20, consider a flowstream reservoir in which the concentration of this one reactant is maintained at a level n_z by its mass flow, Q_A, into the reactor. In general, n_z will decrease with axial position, z (perpendicular to the plane of the figure), from its reactor-inlet value of n_∞ at $z = 0$ as it becomes depleted by the film deposition. Just over the film surface at y = 0, the reactant concentration has dropped to some lower level, n_o. For steady-state deposition and negligible film re-evaporation, the diffusion flux toward the surface, J_A atoms/cm^2·s, will be equal to the film deposition flux, J_r. Approximating dn_A/dy in Fick's law by the n_A difference across the boundary layer, δ_n, we obtain

$$J_r = J_A = -D\frac{n_z - n_o}{\delta_n} \qquad (7.51)$$

or for the fractional depletion of reactant at the surface,

$$f_o = \frac{n_z - n_o}{n_z} = \left| \frac{J_r}{Dn_z/\delta_n} \right| \qquad (7.52)$$

There are two limiting cases of Eq. (7.52), and it is important to know which one applies to the CVD process being run:

1. reaction control: $f_o \to 0$, $n_o \approx n_z$, and $J_r << Dn_z/\delta_n$
2. diffusion control: $f_o \to 1$, $n_o \to 0$, and $J_r \approx Dn_z/\delta_n$

These cases are illustrated in Fig. 7.20, along with an intermediate case. The intermediate case is more difficult to analyze, but since it is also more difficult to control, it should be avoided in CVD practice anyway. Reactors in which the uniformity of reactant flow over the substrate is poor, such as the batch reactor of Fig. 7.5*c*, need to operate under reaction control to achieve uniformity. On the other hand, when surface-T uniformity is hard to achieve, as in the axisymmetric reactor of Fig. 7.5*a*, the exponential dependence of reaction rate on T means that better uniformity is obtainable under diffusion control.

One way to determine whether a process is controlled by reaction or diffusion is to estimate the quantities in Eq. (7.52). The linear deposition rate, dh/dt (nm/s), is easily measured either by thickness deposited in a given time or continuously by ellipsometry or interferometry (Sec. 4.8.2), and it is easily converted to J_r by Eq. (2.21). D often can be found in handbooks or estimated from the formula in Table 2.1. The amount by which n_z is less than the inlet value, n_∞, can be found from the value of J_rA_r (mc/s) compared to Q_A (in mc/s). Here, A_r is the total deposition area *upstream* of the z position being considered; this includes all of the area heated to deposition T, not just the substrate area (see Exercise 7.12). Note that the depletion at z is less than the total fractional utilization of reactant, η, which is determined from n_z at the outlet. In the case of the axisymmetric reactor, η may be large, but the depletion in the flowstream over the substrate is still small, since that region is upstream of the deposition region. For the other reactors in Fig. 7.5, η must be kept small to ensure deposition uniformity, as we shall see below. Consequently, for present purposes we may take $n_z \approx n_\infty$.

The most uncertain quantity in Eq. (7.52) is δ_n. For the axisymmetric reactor with stationary substrate, it might be taken as δ_{vz} from Eq. (7.15), since that is where the flowstream begins to stagnate. However, if the substrate is rotating, δ_n is likely to be less than the δ_{vz} of Eq. (7.20), since the radial flow carrying fresh reactant is actually *increasing* as it approachs the substrate, as shown by curve F in Fig. 7.11. For the tube reactor (Fig. 7.5*b*), the solution for δ_n versus z will be presented below. For the batch reactor (Fig. 7.5*c*), δ_n is the entire distance from substrate edge to center, since there is negligible convective flow between substrates.

Another way to distinguish the reaction- and diffusion-controlled regimes is to measure deposition flux, J_r, versus T. The behavior of this function can be seen by considering the simple case of an irreversible first-order film-forming reaction and a surface coverage $n_s <<$ 1 ML in the linear portion of the adsorption isotherm [Eq. (7.46)] where $n_s \propto n_o$, n_o being the gas-phase reactant concentration just over the surface. Then,

$$J_r = k_s n_s \approx k_a n_o \qquad (7.53)$$

where the rate constant k_a here has units of cm/s. Setting this J_r equal to Eq. (7.51), solving for n_o, and substituting back into Eq. (7.53), we have

$$J_r = \frac{k_a n_z}{1 + \frac{k_a}{D/\delta_n}} \qquad (7.54)$$

which has the following limiting values:

1. reaction control: $k_a << D/\delta_n$ and $J_r \to k_a n_z$
2. diffusion control: $k_a >> D/\delta_n$ and $J_r \to Dn_z/\delta_n$

Since $\log k_a \propto 1/T_s$ with a slope of $-E_a/R$ by Eq. (7.35), where T_s is the surface T in K, such an "Arrhenius plot" for a reaction-controlled process yields a steep straight line as shown for segment (1) of Fig. 7.21. As k_a becomes larger with increasing T_s, diffusion control eventually takes over in segment (2). There, the much smaller slope is determined by the relatively small combined T dependencies of D, n_z, and δ_n. Sometimes, the slope in the reaction-controlled region changes

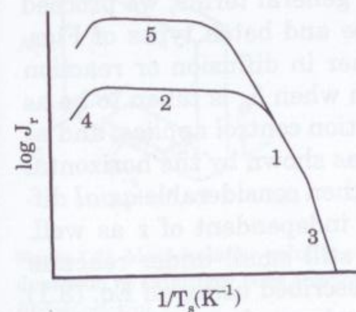

Figure 7.21 Arrhenius-plot behavior of deposition rate. Segments (1) and (3) are reaction-rate controlled with two different E_a values, whereas segments (2) and (5) are diffusion controlled at two different pressures.

with T as shown by segment (3), and this indicates a change in the rate-limiting reaction step to one with a higher E_a. In the special case of a reaction which has marginally negative $\Delta_r G^\circ$ and which is also endothermic, the steep slope may instead represent the equilibrium constant shift toward product [30] with increasing T [Eq. (7.37)]. The slope reversal at high T in segment (4) may indicate either the onset of an equilibrium limit for an exothermic reaction, or the onset of film re-evaporation [Eq. (5.8)]. In general, one must be cautious in the interpretation of Arrhenius plots when thermodynamic and kinetic backup data are unavailable.

The effect of reactor total pressure, p, on deposition flux, J_r, depends on the extent of diffusion or reaction control and on whether it is the reactant's mole fraction, x_A (= n_A/n = p_A/p), or its concentration, n_A ($\propto p_A$), which is held constant as p is varied. The value of x_A can be held constant by increasing p with a fixed gas-flow ratio, using pump throttling at valve b′ in Fig. 7.2. Then n_A (=n_z) increases, and in the reaction-controlled regime, J_r increases per Eq. (7.54). In the diffusion-controlled regime, on the other hand, the 1/p dependence of D cancels out the n_A increase and leaves J_r *independent* of p. However, it is difficult to keep x_A constant over a wide range of p, because at low p, n_A becomes too low for reasonable deposition rate, and at high p it becomes so high that homogeneous reaction to powder can occur, as discussed prior to Eq. (7.41). Therefore, it is more common to keep n_A constant by increasing reactant dilution with increasing p. In that case, J_r is independent of p in the reaction-controlled regime, but it increases with decreasing p in the diffusion-controlled regime because of the increase in D, as shown by segment (5) in Fig. 7.21. This increase in the D-limited J_r is the main reason to operate CVD at reduced p, because it allows reaction-controlled deposition at higher J_r so as to maintain uniformity with reasonable deposition rate in batch reactors.

7.4.2 Reactor models

Having now outlined diffusion behavior in general terms, we proceed to model specific reactors, namely the tube and batch types of Figs. 7.5*b* and *c*. Tube reactors can operate either in diffusion or reaction control. If f_o in Eq. (7.52) is still small even when δ_n is taken to be as large as the entire tube diameter, then reaction control applies, and n_z may be assumed constant across the tube, as shown by the horizontal line in Fig. 7.20. If f_o is *very* small (< 10^{-2}), then considerable *axial* diffusion will also occur, and n_z will become independent of z as well. More commonly though, axial diffusion is still small under reaction control. Then, reactant transport may be described using an Eq. (3.1) mass balance on an axially differential (dz) volume element of uniform

n_z across the reactor's cross section, as shown in Fig. 7.22*a* for a rectangular cross-sectional area, A_t, and for deposition occurring on area A_z per unit length in z. Since the lateral diffusional mixing is fast, the velocity profile across A_t does not matter, and we may use the "plug-flow" assumption of uniform velocity at the mean value, $\bar{u}$, as we did for the oil backstreaming problem in Eq. (3.14) and Fig. 3.4*b*. For first-order reaction kinetics and low surface coverage, where the reactant sticking coefficient, S_c, is independent of n_z, it can be shown (Exercise 7.14) that the reactant depletes exponentially with increasing z according to

$$\frac{n_z}{n_\infty} = \exp\left[-\left(\frac{A_z}{A_t}\right)\sqrt{\frac{T}{M}}\left(\frac{3637 S_c}{\bar{u}}\right)z\right] \quad (7.55)$$

for units of g, cm and s. Under these conditions, the fraction n_z/n_∞ and thus the reactant utilization fraction, η, must be kept small to obtain deposition-rate uniformity over the length of the reactor, unless a compensating $T_s(z)$ gradient is imposed to increase S_c along z. This transport situation may be thought of equivalently as a volume element of unit length in z moving through the reactor at velocity $\bar{u}$ and depositing material out at the periphery as it proceeds. Then, n_z depletes exponentially in time (and thus in z) within the volume element. This behavior is analogous to the exponential pumpout situation of Eq. (3.11).

When diffusion is too slow to maintain reactant concentration at a uniform level n_z across the tube reactor, the volume element shown in Fig. 7.22*b* must be used instead for the mass balance. This element is differential in both y and z, so the u profile in y must now be consid-

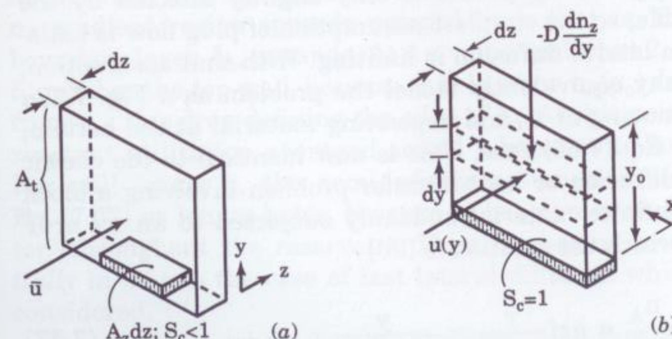

Figure 7.22 Mass-balance volume elements for determining reactant depletion in axial-flow tube reactors: (*a*) reaction control and (*b*) diffusion control.

ered. The net convective flow of reactant A into the element in the z direction, per unit width in x, is $-u(\partial n_A/\partial z)dzdy$. The net diffusive flow into the element in the y direction is

$$\left(-D\,\frac{\partial(\partial n_A/\partial y)}{\partial y}\right)dy\,dz$$

In steady state, n_A is constant in the volume element, so

$$u(y)\,\frac{\partial n_A(y,z)}{\partial z} = D\,\frac{\partial^2 n_A(y,z)}{\partial y^2} \tag{7.56}$$

This illustrates the general procedure for modeling multidimensional flow in CVD reactors. In some cases, gradients in x must also be considered. Such a mass balance must be satisfied for every species in every dxdydz volume element. When homogeneous reactions are occurring, the balance must also include the rates of generation and consumption of every reacting species. Usually, solutions can only be obtained numerically. However, an analytical solution can be obtained for the Fig. 7.22*b* geometry when the u(y) profile is assumed to be either flat or linear [35], and these solutions are shown in Fig. 7.23 using normalized coordinates. The assumed linear u(y) profile approximately tracks the actual parabolic one where the n_A gradient is steep ($y < 0.3y_o$), as shown by the inset. The boundary conditions assumed are: uniform $n_A = n_\infty$ for $z = 0$, $n_A = 0$ at $y = 0$, and no deposition at the top of the reactor ($dn_A/dy = 0$ at $y = y_o$) or on the sides (no flux in the x direction).

Figure 7.23 provides valuable insight into diffusion-limited CVD behavior. Surprisingly, the n_A profile is only slightly affected by the choice of u(y) profile, so the simplest assumption of plug flow is satisfactory even when lateral diffusion is limiting. With that assumption, by the way, we may equivalently model the problem as a Fig. 7.22*a* volume element moving at $\bar{u}$ and depositing material at the bottom, as we did for the Eq. (7.55) case. This is now identical to the classic one-dimensional diffusion or heat-transfer problem involving a block of uniform semi-infinite material suddenly subjected to an n_A or T drop at $y = 0$, for which the solution is [36]

$$\frac{n_A}{n_\infty} = \mathrm{erf}\,\frac{y}{2\sqrt{Dt}} = \frac{y}{2\sqrt{Dz/\bar{u}}} \tag{7.57}$$

Note that the denominator of the error-function (erf) argument is equivalent to the diffusion length, Λ, from Eq. (5.25). Returning now

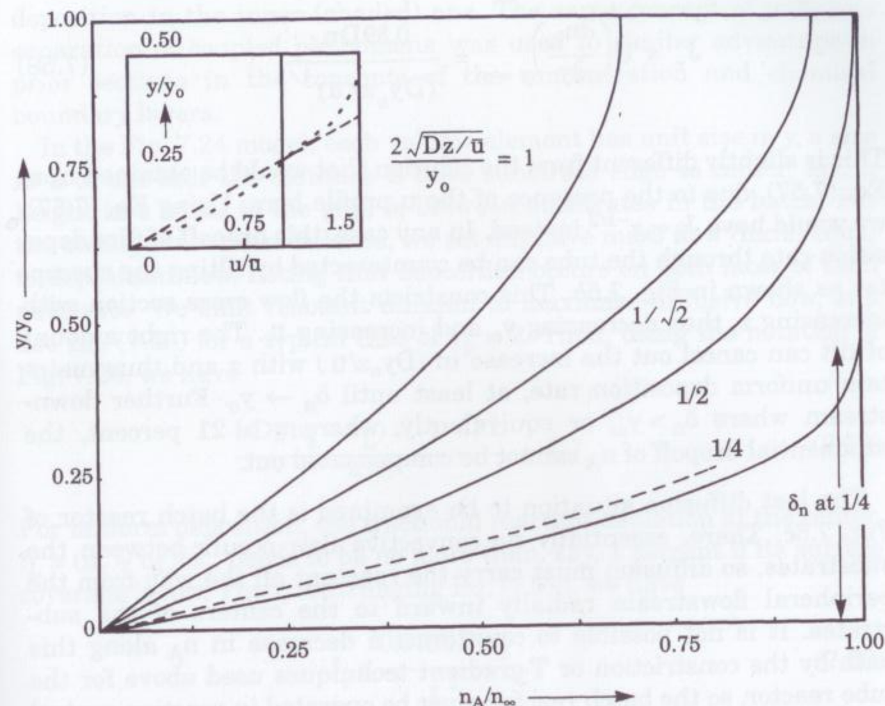

Figure 7.23 Diffusion-limited reactant concentration profiles for four successive normalized axial positions in a tube reactor: solid line = plug flow, long dashes = linear u profile, and short dashes in inset = parabolic profile. (Source: Reprinted from Ref. 35 by permission; curve labeling changed to conform to text.)

to Fig. 7.23, note that as z increases [or t in the Eq. (7.57) model], the n_A-gradient region spreads upward in y; that is, the concentration boundary layer, δ_n, expands. At a z value such that $2\sqrt{Dz/u}/y_o = 1/2$, δ_n reaches the top wall, because that is when $n_A(y_o)$ drops by 1 percent from n_∞, this drop defining the edge of δ_n. At this point, the fractional reactant utilization averaged across y happens to be $\eta = 21$ percent. For still larger z, the semi-infinite assumption breaks down and Eq. (7.57) no longer holds, because δ_n has now spread across the reactor (throughout the reservoir). Then, n_A begins to deplete *exponentially* in z as in the case of fast lateral diffusion which we previously considered.

For smaller z, where $\delta_n < y_o$, the deposition flux, J_r, still decreases with increasing z, because the expansion of δ_n reduces the n_A gradient at the substrate, as seen in Fig. 7.23. It can be shown [35] that for the linear u(y) profile and for $n_A = 0$ at $y = 0$,

$$J_r = D\left(\frac{\partial n_A}{\partial y}\right)_{y=0} = \frac{0.89 D n_\infty}{(D y_o z/\bar{u})^{1/3}} \tag{7.58}$$

This is slightly different from the solution that would be obtained from Eq. (7.57), due to the presence of the u profile here. Using Eq. (7.57), we would have $J_r \propto z^{-1/2}$ instead. In any case, this dropoff of film deposition rate through the tube can be counteracted by tilting the susceptor as shown in Fig. 7.5*b*. This constricts the flow cross section with increasing z, thus decreasing y_o and increasing $\bar{u}$. The right amount of tilt can cancel out the increase in $(D y_o z/\bar{u})$ with z and thus maintain uniform deposition rate, at least until $\delta_n \to y_o$. Further downstream where $\delta_n > y_o$, or equivalently, where $\eta > 21$ percent, the exponential dropoff of n_A cannot be compensated out.

The last diffusion situation to be examined is the batch reactor of Fig. 7.5*c*. There, essentially no convective flow occurs between the substrates, so diffusion must carry the reactant all the way from the peripheral flowstream radially inward to the centers of the substrates. It is not possible to counteract a decrease in n_A along this path by the constriction or T-gradient techniques used above for the tube reactor, so the batch reactor must be operated in reaction control to obtain uniformity. We need to determine how high the deposition rate can be before n_A depletion causes an unacceptable drop in deposition rate at the substrate center. The exact solution to this problem involves integration over radially differential volume elements within which both diffusion and deposition are occurring. However, a considerable simplification which is nevertheless quite accurate enough for present purposes can be made by using only two volume elements and by considering the diffusion to be one-dimensional rather than radial, as shown in Fig. 7.24 by the two dashed rectangles. It is supposed that only diffusion occurs in the outer (left-hand) element, and only

Figure 7.24 Batch-reactor model for diffusion and deposition between stacked substrates of half-width L and arbitrary y dimension; view looking down on a substrate and along the axis of the reactor tube, z.

deposition in the inner (shaded) one. The same concept of judicious separation of coupled phenomena was used to similar advantage in prior sections in the concepts of the concentration and chemical boundary layers.

In the Fig. 7.24 model, each volume element has unit size in y, a size in x of one-half the distance L from substrate edge to center, and a height in z equal to the gap, b, between substrates in the batch. For the steady-state mass balance, we set diffusive mass flow (mc/s) equal to deposition flow, noting that deposition occurs on both faces of each substrate. We omit reactant dilution to maximize diffusive flow, and use Eq. (7.50) for a typical case of $\nu_p = 2$. Then, using the notation of Fig. 7.24, we have

$$\frac{bD(n_z - n_L)/(1/2)L}{4/3} = LJ_r \tag{7.59}$$

For uniform deposition, the fractional reactant depletion at the center, $f_L = (n_z - n_L)/n_z$, needs to be no more than, say, 1 percent if its surface coverage is low. Then, rearranging Eq. (7.59), we have

$$J_r \le \frac{0.015 b D n_z}{L^2} \tag{7.60}$$

Note that the upper limit of J_r is strongly dependent on substrate size, L, but is independent of pressure, p, since $n_z \propto p$ but $D \propto 1/p$. Of course, p must usually be <<1 atm when operating undiluted, to avoid powder formation. Taking typical conditions of b = 1 cm, L = 10 cm, T = 800 K, and D = 0.7 cm^2/s at room T and 1 atm, scaled to 800 K by the Table 2.1 formula, we find that $J_r \le 5\times10^{15}$ atoms/$cm^2\cdot s$ or 1 nm/s, a respectable deposition rate. This is a simple procedure for roughly estimating the range of conditions suitable for operating a batch reactor.

7.4.3 Temperature gradients

Two significant perturbations to diffusion behavior occur in T gradients such as that over the substrate surface. One is "thermal diffusion," which causes the heavier and/or larger of the two molecular species in an A-B mixture to become depleted from the hot region. (In liquids but not in gases, this is known as Soret diffusion.) This behavior is described by the following equation [37], whose derivation is too involved to give here:

$$\frac{dx_A}{dy} = -\left(\frac{D_T}{D_{AB}}\right)\frac{1}{T}\frac{dT}{dy} = -\frac{k_T}{T}\frac{dT}{dy} \tag{7.61}$$

where D_T is the thermal-diffusion coefficient, and k_T is the thermal-diffusion ratio for the mixture. Measured values of k_T are ~0.2, give or take a factor of five for various mixtures [34, 37], but k_T is not easily predicted. It increases with the M differences and diameter differences of the molecules in the mixture, and decreases with increasing molecular interaction. It vanishes for M differences of <10 percent and for x_A or $x_B < 0.1$.

A qualitative picture of the thermal-diffusion effect can be developed using an argument similar to that used to derive the thermal-transpiration effect, Eq. (3.18). Consider the molecular flux of each species along the T gradient as it crosses some plane in space that is perpendicular to the gradient. The flux in each direction arrives at the plane from about one mean free path away toward the hot (T_h) or cold (T_c) end, and the flux is proportional to $p_i/\sqrt{M_i T}$ in accordance with the Knudsen equation [Eq. (2.19)], where i = A or B. If the initial composition is uniform along the gradient ($p_{ih} = p_{ic}$ with total p constant), then Eq. (2.19) results in a net flux, ΔJ_i, for each species toward the hot end. The ratio of these net fluxes is

$$\frac{\Delta J_A}{\Delta J_B} = \frac{J_{Ah} - J_{Ac}}{J_{Bh} - J_{Bc}} = \frac{\dfrac{p_{Ah}}{\sqrt{M_A T_h}} - \dfrac{p_{Ac}}{\sqrt{M_A T_c}}}{\dfrac{p_{Bh}}{\sqrt{M_B T_h}} - \dfrac{p_{Bc}}{\sqrt{M_B T_c}}} = \frac{p_A}{p_B}\sqrt{\frac{M_B}{M_A}} \tag{7.62}$$

If this flux ratio were equal to the p_i ratio, the situation would amount simply to an initial bulk motion of the mixture toward the hot end as in thermal transpiration. However, the flux ratio is seen to be smaller than the p_i ratio when $M_A > M_B$, so that the heavier species has an insufficient net flux and begins to segregate toward the cold end until a steady state is achieved. This segregation can significantly change reactant fluxes to the surface in CVD [38].

The second T-gradient effect is "thermophoresis," which causes small particles suspended in gas to be driven from the hot end [39], just as large molecules are. When the molecular fluxes have reached steady state and when the particle is small enough so that these fluxes can communicate with each other around it (Kn ≥ 1 based on the particle diameter), we must have equal opposing fluxes ($J_h = J_c$) along the gradient. Again, application of the Knudsen equation leads to

$$\frac{p_h}{\sqrt{T_h}} = \frac{p_c}{\sqrt{T_c}} \tag{7.63}$$

That is, p is higher against the hot face of the particle than against the cold face, and the particle is thus pushed toward the cold end. This is identical to the thermal-transpiration equation, Eq. (3.18).

Thermophoresis is a very valuable though generally unappreciated phenomenon in CVD. It is extremely effective in preventing particles homogeneously nucleated within the chemical boundary layer from settling on the film surface. They instead remain suspended within the boundary layer above the substrate and are eventually swept away in the flowstream. Scattering of laser light can be used to dramatically reveal this suspended layer. Particle rejection from the surface is so effective that I have seen quantum-well laser structures (Sec. 6.2.1) successfully grown on a routine basis under MOCVD conditions where such particles were present in abundance. Excessive homogeneous nucleation still causes other problems, however, such as parasitic consumption of source gas and contamination of the reactor with dust.

7.5 Conclusion

CVD is the most complex deposition process which we have examined, due to the many phenomena occurring simultaneously and nonuniformly in the gas phase, namely, forced convection, free convection, homogeneous reaction, and diffusion. Nevertheless, by proper reactor design and operation, it is possible to control each of these phenomena and also to separate their spatial regimes for modeling purposes. Such control provides the surface-chemistry and deposition-rate stability needed to exploit the potential advantages of working with gaseous source materials in the fluid-flow regime. The low sticking coefficient characteristic of gaseous reactants facilitates the coating of convoluted or even porous substrates, or large batches of odd shapes. It also assists selective deposition. The higher pressure of the fluid-flow regime simplifies or eliminates pumping, increases chemistry control latitude because of the higher reactant concentrations, and permits operation under diffusion control for improved film uniformity in the presence of substrate-T nonuniformity. The high T required for activation of most CVD reactions can exceed the tolerance of some substrates, but then one can turn to plasma-enhanced CVD to activate the reactions at lower T, as we will see in Sec. 9.6.

7.6 Exercises

7.1 Reactant gas is flowing into a 1500 cm^3 room-T reactor at 200 sccm as measured on a mass flow controller calibrated for Ar. With the reactor valved off at the outlet, the rate of pressure

rise is 1 torr/s. (a) What is the actual flow rate of the reactant gas in sccm? (b) What is the c_v of the reactant gas?

7.2 For steady-state, one-dimensional laminar flow between parallel plates positioned in the x-z plane at $+y_o$ and $-y_o$, show that the fluid's velocity profile, u(y), is given by Eq. (7.8) and that the mean velocity, $\bar{u}$, is given by Eq. (7.9).

7.3 Show that the thickness of the velocity boundary layer in axisymmetric flow scales as $(T/p^2)^{1/4}$ for a fixed flow velocity at the room-T inlet of the reactor.

7.4 Show that the last equality in Eq. (7.21) for Gr holds assuming the ideal-gas law, and show that it is dimensionless.

7.5 Name at least six ways of suppressing recirculating roll cells in the CVD-reactor gas-flow pattern.

7.6 Show how the chemical-equilibrium equation, Eq. (7.28), is obtained from the G minimization of Eq. (7.27).

7.7 BCl_3 at a partial pressure of 10^3 Pa in 1 atm of H_2 is supplied to an APCVD reactor for the deposition of B at 1400 K. If the only significant gas-phase reaction produces $HBCl_2$ and HCl and reaches equilibrium, what is the fractional conversion of BCl_3? (Use the data of Fig. 7.13)

7.8 The two common forms of arsenic vapor, As_4 and As_2, are in equilibrium with each other in an Ar diluent. (a) Derive the expression for the As_2 partial pressure (in atm) in terms of K, total pressure p, and *initial* p_{Ar}. At the T for which $\Delta_r G° = 0$ and for p = 1 atm, what is the As_2/As_4 partial-pressure ratio for (b) no dilution and (c) for a feed composition of 1 at.% As_4 in Ar?

7.9 A particular deposition reaction operating at 100 Pa and 900 K in a 2-liter isothermal reactor is limited by the unimolecular dissociation, with $k_I = 0.1\ s^{-1}$, of the reactant vapor, which is supplied undiluted at 100 sccm. What fraction, η, of reactant is utilized in the deposition?

7.10 A particular adsorbate, A, of M = 40 is known to have a surface residence time of 1 ms at 1000 K; in other words, the time constant for its desorption when $p_A = 0$ is 1 ms. (a) For a monolayer coverage of $n_{so} = 10^{15}$ mc/cm^2, what is the desorption rate constant in s^{-1}? (b) Assuming Langmuir adsorption kinetics and δ = 1, what p_A is required to sustain a steady-state surface coverage of 90 percent of a monolayer?

7.11 If the Si deposition rate from SiH_4 at 1000 K is being controlled by H_2 desorption at $\Theta \approx 0.9$ in a furnace-type batch reactor, how much of a T increase is needed from the first to the last substrate along the gas flow path to maintain deposition rate uniformity if the SiH_4 utilization is 20 percent? (See data in Sec. 7.3.3.)

7.12 Si is being deposited at 10 nm/min in an isothermal reactor of 2 m^2 total internal-surface area. If SiH_4 is supplied at 200 sccm, what is its fractional utilization, η?

7.13 An axisymmetric cold-wall reactor operating at 1 atm in a flow of 10 sccm B_2H_6 and 5 slm Ar is depositing B onto a stationary 10-cm-diameter, 1400-K substrate. What is the maximum deposition rate in nm/s determined by diffusion limitations?

7.14 (a) Derive Eq. (7.55) using the stationary mass-balance volume element of Fig. 7.22*a*, Eq. (2.18) for the impingement rate of reactant, the ideal-gas law, and the other assumptions stated for Eq. (7.55). (b) Show that the same result is obtained using a volume element moving at the axial flow velocity. (c) For pyrolytic-graphite deposition from methane flowing at 600 sccm and 1300 Pa through a 1-cm-inside-diameter, 1400-K, isothermal tube, what is the length of tube at which the methane will be 20 percent depleted if $S_c = 10^{-4}$?

7.15 It is desired to coat the internal-surface area of porous ceramic catalyst pellets with Pt for application in crude-oil hydrogenation. Assume that this is to be done by CVD from $Pt(CO)_2Cl_2$ at 800 K, and that the pores can be modeled as cylinders 20 nm in diameter and 1 mm long. Using a model similar to that of Fig. 7.24 and the molecular-flow-conductance equation [Eq. (3.6)] adjusted for T and M, determine the maximum S_c to obtain 10 percent coating uniformity from pellet surface to center.

7.16 The units of a reaction rate constant depend on the units of the reactant and the order of the reaction, and one must be careful to use consistent units. What are the SI units of k_a in Eq. (7.46)?

7.7 References

1. Pierson, H.O. 1992. *Handbook of Chemical Vapor Deposition*. Park Ridge, New Jersey: Noyes Publications.
2. Galasso, F.S. 1991. *Chemical Vapor Deposited Materials*. Boca Raton, Fla.: CRC Press.
3. Hinkle, L.D., and C.F. Mariano. 1991. "Toward Understanding the Fundamental Mechanisms and Properties of the Thermal Mass Flow Controller." *J. Vac. Sci. Technol.* A9:2043.
4. Houng, Y.-M. 1992. "Chemical Beam Epitaxy," *Crit. Rev. in Solid State and Mater. Sci.* 17:277.
5. Shealy, J.R., and J.M. Woodall. 1982. "A New Technique for Gettering Oxygen and Moisture from Gases Used in Semiconductor Processing." *Appl. Phys. Lett.* 41:88.
6. Fitzjohn, J.L., and W.L. Holstein. 1990. "Divergent Flow in Chemical Vapor Deposition Reactors." *J. Electrochem. Soc.* 137:699.
7. Schlichting, H. 1968. *Boundary-Layer Theory*, 6th ed. New York: McGraw-Hill, Chap. V.

8. Breiland, W.G., and G.H. Evans. 1991. "Design and Verification of Nearly Ideal Flow and Heat Transfer in a Rotating Disc Chemical Vapor Deposition Reactor." *J. Electrochem. Soc.* 138:1806.
9. McAdams, W.H. 1954. *Heat Transmission*, 3rd ed. New York: McGraw-Hill, Chap. 7.
10. Giling, L.J. 1982. "Gas Flow Patterns in Horizontal Epitaxial Reactor Cells Observed by Interference Holography." *J. Electrochem. Soc.* 129:634.
11. Chase, M.W., et al. (eds.) 1985. *JANAF Thermochemical Tables*, 3rd ed. Washington, D.C.: American Chemical Society.
12. Wagman, D.D., et al. (eds.). 1982. "NBS Tables of Chemical Thermodynamic Properties," *J. Phys. Chem. Ref. Data* 11, suppl. no. 2.
13. Bernard, C., and R. Madar. 1990. "Thermodynamic Analysis and Deposition of Refractory Metals." In *Proc. Chemical Vapor Deposition of Refractory Metals and Ceramics Symp.* 168:3. Pittsburgh, Pa.: Materials Research Society. These authors recommend the following on-line services: F.A.C.T., Facility for the Analysis of Chemical Thermodynamics, Ecole Polytechnique, Montreal, Québec, Canada; IVTANTHERMO, Institute of High Temperature of the Russian Academy of Sciences, Moscow; THERMODATA, Domaine Universitaire de Grenoble, BP.66, 38402 Saint Martin d'Hères cedex, France; and THERMO-CALC DATA BANK, Royal Inst. of Technol., S-10044, Stockholm, Sweden.
14. Besmann, T.M. 1977. "SOLGASMIX-PV, a Computer Program to Calculate Equilibrium Relationships in Complex Chemical Systems," ORNL/TM-5775. Oak Ridge, Tennessee: Oak Ridge National Laboratory.
15. McNevin, S.C. 1986. "Chemical Etching of GaAs and InP by Chlorine: The Thermodynamically Predicted Dependence on Cl_2 Pressure and Temperature." *J. Vac. Sci. Technol.* B4:1216.
16. Skelly, D.W., T.-M. Lu, and D.W. Woodruff. 1987. "Metallization Techniques," Chap. 3 in *VLSI Metallization*, vol. 15 of *VLSI Electronics and Microstructure Science*, ed. N.G. Einspruch, S.S. Cohen, and G. Sh. Gildenblat. Orlando, Fla.: Academic Press.
17. Spear, K.E., and R.R. Dirkx. 1990. "Predicting the Chemistry in CVD Systems." In *Proc. Chemical Vapor Deposition of Refractory Metals and Ceramics Symp.* 168:19. Pittsburgh, Pa.: Materials Research Society.
18. Jasinski, J.M., and S.M. Gates. 1991. "Silicon Chemical Vapor Deposition One Step at a Time: Fundamental Studies of Silicon Hydride Chemistry." *Accts. Chem. Res.*, 24:9.
19. Jasinski, J.M. 1994. "Gas Phase and Gas Surface Kinetics of Transient Silicon Hydride Species." In *Gas-Phase and Surface Chemistry in Electronic Materials Processing*. Pittsburgh, Pa.: Materials Research Society.
20. Holleman, J., and J.F. Verweij. 1993. "Extraction of Kinetic Parameters for the Chemical Vapor Deposition of Polycrystalline Silicon at Medium and Low Pressures." *J. Electrochem. Soc.* 140:2089.
21. Qian, Z.M., H. Michiel, A. Van Ammel, J. Nijs, and R. Mertens. 1988. "Homogeneous Gas Phase Nucleation of Silane in Low Pressure Chemical Vapor Deposition." *J. Electrochem. Soc.* 135:2378.
22. de Croon, M.H.J.M., and L.J. Giling. 1990. "Chemical Boundary Layers in CVD." *J. Electrochem. Soc.* 137:2867.
23. Buss, R. J., P. Ho, W.G. Breiland, and M.E. Coltrin. 1988. "Reactive Sticking Coefficients for Silane and Disilane on Polycrystalline Silicon." *J. Appl. Phys.* 63:2808.
24. Scott, B.A., and R.D. Estes. 1989. "Role of Gas-Phase Reactions in Silicon Chemical Vapor Deposition from Monosilane." *Appl. Phys. Lett.* 55:1005.
25. Toyoshima, Y., K. Arai, A. Matsuda, and K. Tanaka. 1990. "Real Time *in situ* Observation of the Film Growth of Hydrogenated Amorphous Silicon by Infrared Reflection Absorption Spectroscopy." *Appl. Phys. Lett.* 56:1540.
26. Haupfear, E.A., and L.D. Schmidt. 1993. "Kinetics and Multiple Steady States in the Chemical Vapor Deposition of Titanium Carbide." *J. Electrochem. Soc.* 140:1793.
27. Hsieh, J.J. 1993. "Influence of Surface-Activated Reaction Kinetics on Low-Pressure Chemical Vapor Deposition Conformality over Micro Features." *J. Vac. Sci. Technol.* A11:78.
28. Palmer, B.J., and R.G. Gordon. 1988. "Local Equilibrium Model of Morphological Instabilities in Chemical Vapor Deposition." *Thin Solid Films* 158:313.
29. Yew, T-R., and R. Reif. 1989. "Silicon Selective Epitaxial Growth at 800° C using SiH_4/H_2 assisted by H_2/Ar Plasma Sputter." *Appl. Phys. Lett.* 55:1014.
30. Shaw, D.W. 1974. "Mechanisms in Vapour Epitaxy of Semiconductors." Chap. 1 in vol. 1, *Crystal Growth: Theory and Techniques*, ed. C.H.L. Goodman. London: Plenum Press.
31. Hoyt, J.L., C.A. King, D.B. Noble, C.M. Gronet, J.F. Gibbons, M.P. Scott, S.S. Laderman, S.J. Rosner, K. Nauka, J. Turner, and T.I. Kamins. 1990. "Limited Reaction Processing: Growth of $Si_{1-x}Ge_x$/Si for Heterojunction Bipolar Transistor Applications." *Thin Solid Films* 184:93.
32. Houle, F.A. 1989. "Surface Photoprocesses in Laser-Assisted Etching and Film Growth." *J. Vac. Sci. Technol.* B7:1149.
33. Isobe, C., H.C. Cho, and J.E. Crowell. 1993. "Photochemical vs. Thermal Deposition of Group IV Semiconductors." Paper presented at annual Am. Vacuum Soc. Meeting, Chicago, November 1993.
34. Bird, R. B., W.E. Stewart, and E.N. Lightfoot. 1960. *Transport Phenomena*. New York: John Wiley & Sons, 570.
35. Van de Ven, J., G.M.J. Rutten, J.J. Raaijmakers, and L.J. Giling. 1986. "Gas Phase Depletion and Flow Dynamics in Horizontal MOCVD Reactor." *J. Crystal Growth* 76:352.
36. Crank, J. 1975. *The Mathematics of Diffusion*. Oxford, U.K.: Oxford University Press.
37. Grew, K.E., and T.L. Ibbs. 1952. *"Thermal Diffusion in Gases."* Cambridge, U.K.: Cambridge University Press.
38. van Sark, W.G.J.H.M., M.H.J.M. de Croon, G.G. Janssen, and L.J. Giling. 1990. "Analytical Models for Growth by Metal Organic Vapour Phase Epitaxy: II. Influence of Temperature Gradient." *Semicond. Sci. Technol.* 5:36.
39. Talbot, L., R.K. Cheng, R.W. Schefer, and D.R. Willis. 1980. "Thermophoresis of Particles in a Heated Boundary Layer." *J. Fluid Mech.* 101:737.

7.8 Recommended Readings

Benson, S.W. 1968. *Thermochemical Kinetics*. New York: John Wiley & Sons.

Jensen, K.F. 1989. "Transport Phenomena and Chemical Reaction Issues in OMVPE (Organometallic Vapor Phase Epitaxy) of Compound Semiconductors." *J. Crystal Growth* 98:148.

Smith, W.R. 1980. "The Computation of Chemical Equilibria in Complex Systems." *Indust. and Engineering Chem. Fundamentals* 19:1.

Stringfellow, G.B. 1989. *Organometallic Vapor-Phase Epitaxy: Theory and Practice*. Boston, Mass.: Academic Press.